JOURNAL OF GEOPHYSICAL RESEARCH: ATMOSPHERES, VOL. 118, 1–21, doi:10.1029/2012JD018291, 2013

Black carbon and other light-absorbing impurities in snow across Northern China

Xin Wang,[1] Sarah J. Doherty,[2] and Jianping Huang[1]

Received 17 June 2012; revised 8 November 2012; accepted 25 November 2012.

[1] Black carbon (BC), organic carbon (OC), and mineral dust (MD) are the most important light-absorbing particulate impurities in snow. A field campaign was conducted in January and February 2010 to measure light-absorbing particles in snow across northern China. About 400 snow samples were collected at 46 sites in six provinces. A spectrophotometer was used to separate snow particulate absorption by BC and non-BC constituents, based on the different spectral dependences of their light absorption. Light absorption by MD is due to iron oxides, so iron concentration was determined by chemical analysis. Using assumed mass absorption efficiencies for BC, OC, and iron, the fractional contribution of each to total absorption was estimated. BC is a product of combustion and iron is associated with MD, but OC in snow can be associated with either combustion products deposited to snow or from soil mixed into snow. The lowest concentrations of BC were in the remote northeast on the border of Siberia, with a median concentration in surface snow of 117 ng g^{-1}. South of this, in the industrial northeast, the median snow BC concentration was 1220 ng g^{-1}. In the northeast, snow particulate light absorption was dominated by BC. Across the grassland of Inner Mongolia, OC, likely mostly from local soil, dominates light absorption, with median BC concentrations of 340 ng g^{-1} responsible for only about one third of total particulate light absorption. In the Qilian Mountains, at the northern boundary of the Tibetan Plateau, snow particulate light absorption is dominated by local soil and desert dust.

Citation: Wang, X., S. J. Doherty, and J. Huang (2013), Black carbon and other light-absorbing impurities in snow across Northern China, *J. Geophys. Res. Atmos.*, *118*, doi:10.1029/2012JD018291.

1. Introduction

[2] Black carbon (BC) deposited to snow and sea ice reduces the surface albedo and warms climate through the snow-albedo feedback [*Warren and Wiscombe*, 1980; *Hansen and Nazarenko*, 2004; *Jacobson*, 2004; *Flanner et al*., 2007]. Modeling studies have investigated the role of BC in snow, sea ice, and glaciers in the recent warming of the Arctic [*Hansen and Nazarenko*, 2004; *Jacobson*, 2004; *Flanner et al*., 2007, 2009; *Koch et al*., 2009a; *Shindell and Faluvegi*, 2009], decreasing springtime snow cover in Eurasia [*Flanner et al*., 2009] and on warming and the hydrologic cycle in the western U.S. [*Qian et al*., 2009] and in the Tibetan Plateau/Himalayan region [*Qian et al*., 2011; *Kopacz et al*., 2011]. However, modeled atmospheric distributions of BC vary widely and, when compared to observations, have significant biases [*Koch et al*., 2009b; *Schwarz et al*., 2010]. This indicates that modeled deposition of BC is also highly uncertain. Indeed, *Hansen et al*. [2005] identified BC in snow and ice as one of the largest sources of uncertainty in their comprehensive assessment of the various radiative forcings of climate change.

[3] Model representation of snow and ice BC concentrations in the Arctic can be tested using a geographically broad set of field measurements [*Clarke and Noone*, 1985; *Chýlek et al*., 1987; *Cachier and Pertuisot*, 1994; *Chýlek et al*., 1995; *Hagler et al*., 2007a, 2007b; *McConnell et al*., 2007; *Grenfell et al*., 2002; *Forsström et al*., 2009; *Doherty et al*., 2010]. However, until now observations of BC in seasonal snow at mid-latitudes have been limited to studies focusing on a few sites in North America [*Clarke and Noone*, 1985; *Chýlek et al*., 1987; *Cadle and Dasch*, 1988; *Dasch and Cadle*, 1989], Europe [*Sergent et al*., 1993, 1998; *Fily et al*., 1997; *Armalis*, 1999], and on glaciers in Tibet [*Xu et al*., 2006, 2009, 2012; *Ming et al*., 2008, 2009]. Here we present measurements of BC and other light-absorbing particles in snow from 46 sites widely distributed across north-central and northeast China from January and February 2010.

[4] Combustion-generated BC is the most important anthropogenic particulate light absorber for solar radiation [*IPCC*, 2007], and BC has been the focus of most mid-latitude snow measurements to date. However, organic carbon (OC)

[1]Key Laboratory for Semi-Arid Climate Change of the Ministry of Education, College of Atmospheric Sciences, Lanzhou University, Lanzhou, China.
[2]Joint Institute for the Study of Atmosphere and Ocean, University of Washington, Seattle, Washington, USA.

Corresponding author: J. Huang, Key Laboratory for Semi-Arid Climate Change of the Ministry of Education, College of Atmospheric Sciences, Lanzhou University, Lanzhou, China. (hjp@lzu.edu.cn)

2169-897X/13/2012JD018291

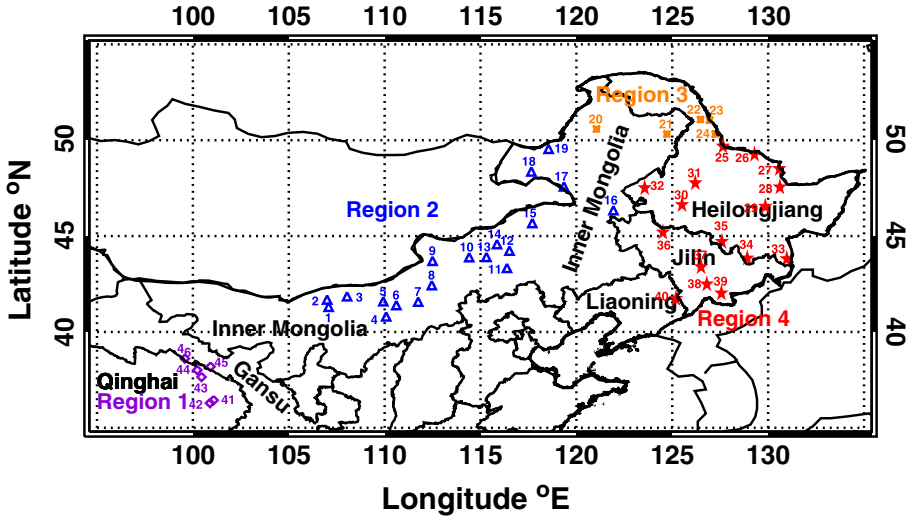

Figure 1. Snow sampling sites across northern China during the 2010 field campaign.

and mineral dust (MD) may also account for a significant fraction of particulate light absorption in snow [*Painter et al*., 2007; *Doherty et al*., 2010]. Light-absorbing organic "brown" carbon and its precursors are coemitted with BC in fossil fuel (FF) combustion, biofuel combustion, and open biomass burning (BB) [*Andreae and Gelencsér*, 2006] and will be deposited to snow along with BC in both dry and wet deposition. Iron in MD, usually in the form of either hematite or goethite, also absorbs solar radiation. The Loess Plateau and the deserts in the arid and semiarid regions of Mongolia and northwest China are considered some of the largest and most persistent dust sources in the Northern Hemisphere [*Prospero et al*., 2002; *Alfaro et al*., 2004; *Wang et al*., 2008, 2010; *Huang et al*., 2007, 2008, 2010], and dust lofted from these deserts can be deposited to snow downwind of source regions, either by settling from the atmosphere or in precipitation. Organics in the form of humic-like substances (HULIS) in soil also absorb solar radiation. Snow cover in north-central China is thin and sometimes patchy, even in mid- to late winter, increasing the likelihood that local soil will mix with the snow. Locally strong winds may loft soil into the atmosphere where it can then settle on snow, or it may be mechanically mixed into the snow, such as by livestock. Therefore, while pollution sources in northeast China are some of the most intense in the world [*Bond et al*., 2004], the proximity of deserts and thin snow cover across much of north China mean that snow albedo in this region may be strongly affected not only by BC, but also by combustion organics, soil organics, and iron oxides in soil and MD.

[5] The primary purposes of this article are to describe the first large-area survey of light-absorbing particles in seasonal snow over northern China, investigate the wavelength dependence of solar light absorption by particulate impurities in snow, and distinguish the contributions to this light absorption by BC, OC, and MD. Also included is a comparison of measured BC concentrations with those predicted in a global model study. A brief report on the China 2010 expedition, with preliminary results, was presented by *Huang et al*. [2011]. The campaign reported on here and by *Huang et al*. [2011] was followed up by a second campaign to measure the BC content in seasonal snow in Qinghai and Xinjiang provinces of western China in January and February 2012 [*Ye et al*., 2012].

2. Method

2.1. Sample Location and Filtration

[6] Snow was sampled at 46 sites across northern China in January–February 2010 (Figure 1). Over most of this area, the snow melts in March, but in the far northeast it remains cold until April. The field season was therefore planned to sample the snowpack close to the time of maximum snow cover, but before melting had commenced at any of the sites. For each site, we collected a vertical profile of samples in order to resolve how particulate light absorption in snow varied through the fall/winter deposition seasons. As Figure 1 shows, the China 2010 field campaign can be grouped into regions. Regions 2–4 include 40 sites sampled in January to early February, going from west to east, in the provinces of Inner Mongolia, Heilongjiang, Jilin, and Liaoning. A subsequent short trip in mid-February included snow sampling at six sites in Qinghai and Gansu provinces (Figure 1, region 1). Sites 41–46 (region 1) are in the Qilian Mountains on the Qinghai/Gansu border, the northeast part of the Qinghai-Tibet Plateau. Sites 1–19 (region 2) span the northern Inner Mongolian grasslands. A transition to deeper snowpack and proximity to Siberia demarks region 3. Region 4 is distinguished from region 3 in being more heavily industrialized, and emissions within this region are much higher than in the other three regions [*Lu et al*., 2011, Figure 8]. In an effort to have our samples be regionally representative and to minimize the effects of local sources, sampling locations were chosen more than 1 km away from roads and highways and usually at least 50 km from villages and cities. The exception is site 4, where the intent was to see the influence of a nearby city on snow particulate impurities by comparison of these samples to the rest of region 2.

[7] Generally, snow samples were collected at vertical intervals of 5 cm throughout the snowpack depth. However, in Inner Mongolia and the Qilian Mountains, the snow was usually <5 cm deep. For these sites, samples were collected

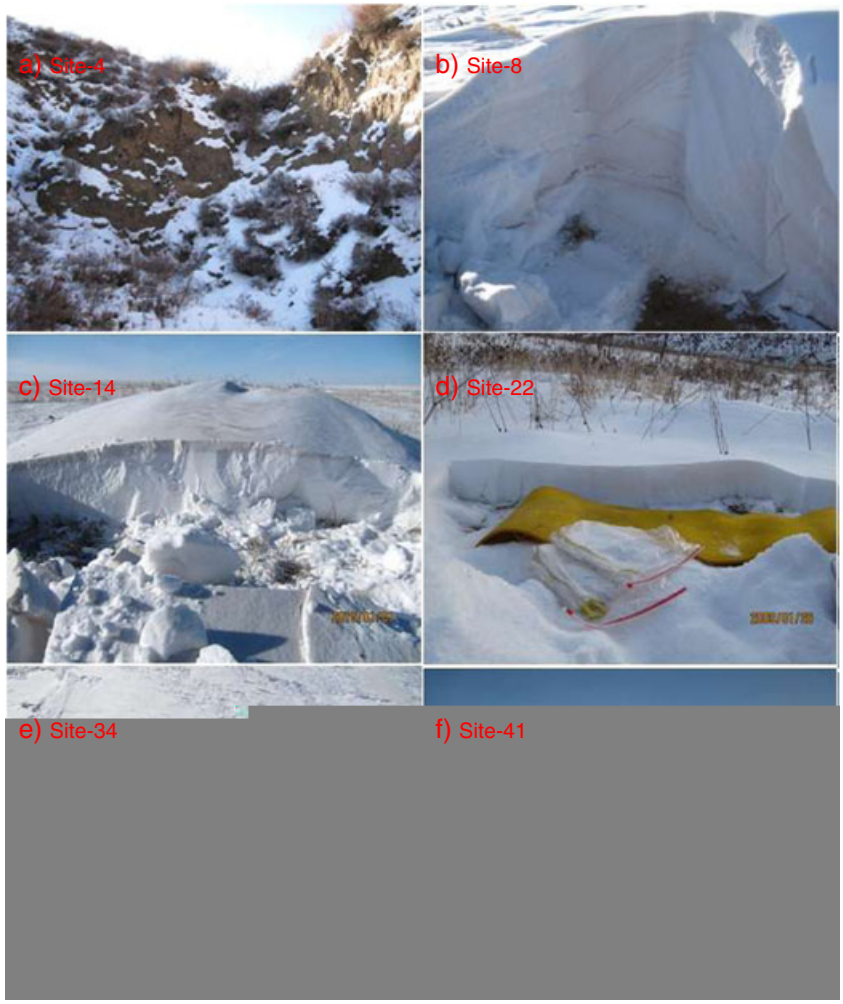

Figure 2. Examples of snow sampling locations at (a) site 4, near Baotou (b) site 8, in the grasslands (c) site 14, in the grasslands (d) site 22, the northern-most and cleanest site (e) site 34, on a lake, and (f) site 41, in the Qilian Mountains of Qinghai province.

from drifted snow, so vertical profiles from these sites are affected by mixing with drifting and will not necessarily represent the seasonal evolution of deposition to snow. This also means that the snow depths of the samples in this region are greater than the typical snow depth. In Heilongjiang province (sites 22–35), snow cover was relatively uniform and sufficiently deep that sampling locations did not need to be selected based on snow depth.

[8] Photos from six sites where snow samples were gathered are shown in Figure 2. Site 4 (Figure 2a) is only 30 km from Baotou, the largest industrial city in the central part of Inner Mongolia. Especially during the winter, air pollution near Baotou is mainly composed of BC and OC caused by BB and coal burning [*Fan et al*., 2008; *Liu et al*., 2009; *Gu et al*., 2010; *Zhao et al*., 2012]. The filters from this site were gray, which is consistent with particle absorption being dominated by BC from FF combustion. Site 8 (Figure 2b) is located southwest of the Erenhot railway in the grasslands of Inner Mongolia. In this region, the snow was thin, so we collected samples from drifted snow, which appears, on visual inspection, to be mixed with local soil. Figure 2c shows site 14, where there was relatively cleaner snow below a visually dirty surface snow layer. Wind-blown soil can be seen on top of the snowdrift. The visually dark top 3 cm in Figure 2c contains high levels of both dust and BC, as discussed below. The cleanest snow measured was in the remote northeast, near 51°N on the border of Siberia. Figure 2d shows site 22, which is the cleanest site of the whole campaign. In contrast, Figure 2e shows site 34, on a lake near the border of Heilongjiang and Jilin provinces, which had relatively large amounts of light-absorbing impurities throughout the snowpack depth. The sites in the Qilian Mountain region at the northern end of the Tibetan Plateau were characterized by very patchy snow (Figure 2f). In addition to likely contamination with local soil, this region is often downwind of the Taklimakan Desert, so the snow probably contains significant amounts of desert MD. Indeed, we will show below that snow iron concentrations were markedly higher in region 1 than in the other three regions.

[9] During snow sampling, we walked at least 1 km from local roads then took care that the sample area remained upwind. Snow was sampled with cleaned, stainless steel utensils and placed in plastic Whirlpak bags until it could be melted and filtered. At all sites, two profiles of samples ("left" and "right") were collected through the whole depth

of the snowpack. Temporary labs were set up in hotels along the sampling route, at Erenhot to process sites 1–11, at Harbin to process sites 12–29, as well as sites 30–35, which were sampled by part of the field team while processing was under way in Harbin, and at Shenyang (sites 36–40). Snow from sites 41–46 was processed at Lanzhou University. Photographs of temporary labs in the field are shown by *Huang et al*. [2011] and *Ye et al*. [2012]. Details of the procedure for melting and filtering the snow samples are given by *Doherty et al*. [2010].

[10] Sample snow was spooned into a clean glass beaker with a clean stainless steel utensil then melted rapidly in a microwave. It is important to minimize the time the melted sample is kept in the container in order to minimize losses of BC and other particles to the container walls [*Ogren et al*., 1983]. Therefore, immediately after melting a measured volume of the sample, meltwater was drawn through 0.4 μm Nuclepore filters, using a hand pump to create a partial vacuum. Approximately 60 mL of sample meltwater from both before and after filtration were also saved into high-density polyethylene bottles and refrozen later for chemical analysis (section 2.2).

[11] Nuclepore filters with a pore size of 0.4 μm were used because filters with a smaller pore size quickly become clogged, and this prevents drawing enough meltwater through the filter to get sufficient loading for analysis with the Integrating Sandwich/Integrating Sphere (ISSW) spectrophotometer [*Grenfell et al*., 2011]. However, filters with this pore size do not capture all snow particulates. An under-catch correction of 15% was determined using samples from a range of locations. The filtrate from the 0.4 μm filters was refiltered through 0.2 μm pore size filters, then both filters were measured with the photometer [*Doherty et al*., 2010]. All reported concentrations have been scaled up by 15% to account for under-catch. The under-catch tests were made on snow samples where combustion sources likely dominated snow particulate matter, so the capture efficiency of larger particles, such as soil and MD, may be higher. Thus, the 15% may be an overcorrection for samples where snow particulate matter is dominated by soil and MD (i.e., sites 1–13 and 41–46).

[12] It was apparent from visual inspection that many snow samples, particularly those from the grasslands of Inner Mongolia and the Qilian Mountains, contained significant amounts of coarse-grained soil. Particles of this size (visually resolved by eye) are derived from local origin and so will not be captured as a source of light absorbing particulates to snow in climate models. Therefore, separation of the contributions to snow by local soil and by regionally or long-range–transported aerosol is useful both in aiding comparisons of our measurements to models and to understanding the sources of light-absorbing particulates to snow. In an attempt to separate particles of local origin versus particles deposited to the snow after regional or long-range transport, for most samples we did two filtrations. "Stirred" samples have been agitated, so all but the very largest particles are captured by the filtration process. For "settled" samples, the snowmelt was left to sit for approximately 3–5 minutes after melting so the larger particles ($> \sim 10\ \mu$m diameter) could settle to the bottom of the glass beaker. The filtration process typically took an additional 3–5 minutes. As noted above, two samples were gathered for each snow layer. For those sites apparently influenced by local soil, both stirred and settled filtrations were done for the left set of samples, and only a settled filtration was done for the right set of samples. Both stirred and settled filtrations were done for most samples from all sites other than 20–27 along the northeast border of China (Figure 1), where the snow was deeper and the influence of coarse-grained soil and sand did not appear significant.

[13] Snow samples were ideally kept frozen in Whirlpak bags until they were melted for filtering. However, samples from sites 12–46 partially or fully melted in transit and then refroze in transit before being intentionally melted for filtration. When these samples were melted in the microwave in a glass beaker, we noticed a ring was left behind near the waterline. When this "scum ring" was wiped with a clean Kimwipe tissue, it was apparent that the ring included light-absorbing particles. Subsequent studies in the lab indicated that the Whirlpak bag interior includes some sort of surfactant that mixes with snow meltwater when the samples are allowed to melt in the bags, and this produces the observed scum ring.

[14] Two sets of data were used to generate a correction factor for losses of light-absorbing particles to the scum for samples from sites 12–46. First, the Kimwipes used to clean the beakers were dried, then kept in clean plastic bags for later analysis in the lab. For a subset (14) of the wipes, particulates were extracted from the wipes using the following procedure: The portion that was noticeably discolored was isolated and cut out with scissors that had been cleaned in methanol. These portions of the wipes were placed in glass sample bottles and immersed in 80% methanol water solution, mechanically agitated for ~5 minutes, then sonicated for 30 minutes at 28°C. The wipes were then removed from the solution and washed with 100% methanol as they were being withdrawn, the wash going into the sample water bottles. The methanol solution was then filtered, following the filtration procedure used for snow samples, and the filters analyzed with the ISSW for particulate light absorption lost to the scum in the snow meltwater.

[15] For a second approach to determining the correction, samples were collected in the mountains of Washington State from a single site using either clean glass jars or Whirlpak bags. Some of these samples were allowed to partially melt in the bag before being intentionally melted in a beaker and filtered for analysis. Loss factors were determined by comparing particulate light absorption in snow sampled directly into glass jars versus that from snow allowed to partially melt in the Whirlpak bags before complete melting in the microwave oven. These tests showed that the losses to scum decreased exponentially as the concentration of light-absorbing impurities increased, presumably because the scum quickly becomes saturated with particles. Using a best fit to the data from the two tests above, a correction factor, S, was determined and applied to all impurity concentrations for sites 12–46, as shown in equation (1):

$$S = 1.508 - 0.16 * \log_{10}\left(C_{BC}^{\max}\right) \quad (1)$$

where $C_{BC}^{\max}$ is a metric for total light absorption from optical analysis (see section 2.3 below). S is ~1.5 for the lowest concentration samples at sites 22 and 23, but, on average, is 1.07 ± 0.07 for the samples across

sites 12–46. At $C_{BC}^{\max}$ = 1500 ng g^{-1}, the correction factor (S) goes to 1 (Figure 3).

2.2. Chemical Speciation

[16] Chemical analysis of snow meltwater followed the procedures described by *Hegg et al.* [2009, 2010]. Inductively coupled plasma optical emission spectrometry and ion chromatography were used to measure concentrations of roughly two dozen chemical species, including standard anions, such as sulfate and nitrate, biomass markers, such as levoglucosan and nonsoil potassium, industrial markers, such as vanadium, and MD markers, such as silicon, iron, and aluminum. Analysis of soluble species was generally done using the filtrate from samples processed for optical analysis (section 2.1) in order to ensure that the optical and chemical analyses were for identical snow sample meltwater. However, for analysis of nonsoluble species (e.g., iron), prefiltered meltwater from the same bulk snow meltwater sample was used and acidified to 0.2 M nitric acid. The full set of chemical data will be used in a positive matrix factorization analysis for source attribution of light-absorbing particles in the snow, paralleling the Arctic analyses of *Hegg et al.* [2009, 2010]. The results of that analysis will be reported in a separate article. Here only the iron concentrations from this analysis are used, to estimate spectrally resolved light absorption in the snow attributable to iron oxides.

2.3. Spectrophotometric Analysis

[17] Filtered snow samples were analyzed for BC and other light-absorbing particles using the ISSW spectrophotometer, described by *Grenfell et al.* [2011] and employed by *Doherty et al.* [2010] for analysis of Arctic snow samples. This technique uses the wavelength dependence of measured spectral light absorption to derive the maximum possible BC concentration, a best estimate of the snow BC concentration, the spectral absorption properties of all light-absorbing particulates in the snow, and the fraction of absorption due to non-BC absorbers. Specifically, it is used to derive the following quantities:

1. C_{BC}^{est} (ng g^{-1}): *estimated BC* is the estimated true mass of BC per mass of snow, derived by separating the spectrally resolved total light absorption.
2. $C_{BC}^{\max}$ (ng g^{-1}): *maximum BC* is the mass of BC per mass of snow, if all particulate light absorption (650–700 nm) is due to BC.
3. C_{BC}^{equiv} (ng g^{-1}): *equivalent BC* is the amount of BC that would need to be present in the snow to account for the wavelength-integrated (300–750 nm) total light absorption of down-welling solar radiation by all particulate constituents.
4. $\AA_{tot}$: *absorption Ångström exponent*, defined below, is calculated between 450 and 600 nm, for all particulate deposited on the filter.
5. f_{nonBC}^{est} : *fraction of light absorption by non-BC light-absorbing particles*, is the absorption by non-BC particulate constituents, weighted by the down-welling solar flux, then spectrally integrated from 300 to 750 nm.
6. $R_{stir,settle}$: the ratio of C_{BC}^{equiv} for the stirred and settled samples. This parameter indicates how much of the spectrally integrated solar absorption by particles in the snowpack are due to very large (>10μm diameter) particles, likely of local origin (i.e., soil).

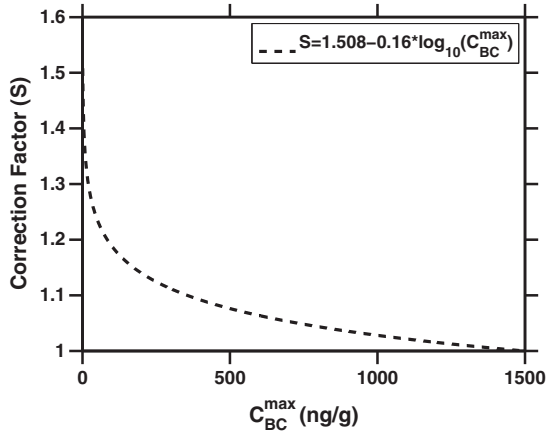

Figure 3. The correction factor (S) to all impurity concentrations for sites 12–46 as a function of $C_{BC}^{\max}$.

[18] The ISSW measures light absorption by all constituents on the sample filters. Absorption by non-BC constituents decreases more rapidly with wavelength than does absorption by BC, so the fraction of total absorption attributable to BC is higher at longer wavelengths (e.g., 650–700 nm) than at shorter wavelengths (<650 nm). Therefore, a maximum possible BC mass ($C_{BC}^{\max}$) is calculated by attributing all of the light absorption at 650–700 nm to BC. A set of calibration standards with a mass absorption efficiency of 6.3 m^{2}g^{-1} at 550 nm is used to convert measured absorption to BC mass loading on the filter (μg/cm^2). The filter loading is converted to a snow concentration by accounting for the filter-exposed area (cm^2) and the mass of snow meltwater drawn through the filter (g), yielding concentrations in ng BC per g snow water (ng·g^{-1}; or, equivalently, ppb). Snow BC concentration is calculated by attributing the 650–700 nm absorption to BC and non-BC constituents, as described below. The equivalent BC mass, C_{BC}^{equiv}, is calculated by weighting the 300–750 nm absorption by the down-welling solar flux, then attributing all of this absorption to BC, thus it is a measure of the amount of BC that would be needed to account for the absorption of solar radiation by all constituents. C_{BC}^{equiv} is larger than $C_{BC}^{\max}$ because it accounts for the relatively stronger absorption at shorter wavelengths by non-BC constituents.

[19] Spectral absorption by particles is primarily a function of particle composition and secondarily of particle size. A common metric for characterizing spectral absorption is the absorption Ångström exponent, $\AA$, which is calculated as the negative of the slope of absorption versus wavelength on a log-log scale. Here $\AA_{tot}$ is $\AA$ for all particulates on the sample filters. We use $\AA_{tot}$ both as an indicator of the source of snow particulate light absorption and as input to our method for separating BC and non-BC particulate absorption (section 2.4). Following common practice, we calculate $\AA_{tot}$ over the wavelength range 450–600 nm.

[20] The mass concentrations, C_{BC}^{est}, $C_{BC}^{\max}$, and C_{BC}^{equiv}, directly depend on the mass absorption efficiency (MAE) of the synthetic BC used for our calibration standards (6.3 m^2 g^{-1} at 550 nm). If the BC in snow actually has an MAE of, for

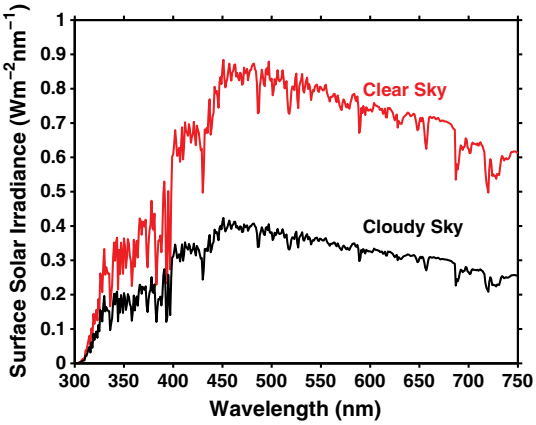

Figure 4. Representative down-welling solar irradiance for north China in winter for clear and fully cloud-covered conditions. The wavelength range is limited to the 300–750 nm band used for the absorption calculations (model calculation provided by Q. Fu, Dept. of Atmospheric Sciences, Univ. of Washington, Seattle, Washington, USA).

example, 7.5 $m^2\ g^{-1}$, our reported mass concentrations will be too high by a factor of 1.19 (but the absorption will be correct if our concentrations are used with MAE = 6.3 $m^2\ g^{-1}$).

[21] Ultimately of interest is how snow albedo is being reduced by light-absorbing impurities. Some, but not all, of this light absorption is due to BC. A metric for the relative roles of BC and non-BC constituents in albedo reduction is the fraction of absorption due to non-BC particulate matter, f^{est}_{nonBC}. The range of the spectral wavelengths used to calculate f^{est}_{nonBC} (300–750 nm) is based on the fact that solar radiation at the surface is negligible below 300 nm and the fact that light-absorbing particles have little effect on snow albedo for wavelengths longer than 750 nm [*Warren and Wiscombe*, 1980]. For this sample set, f^{est}_{nonBC} was calculated using the incident solar irradiance, $F_o(\lambda)$, for clear-sky atmospheric conditions representative of north China in winter (Figure 4); use of the cloudy-sky irradiance yields almost identical results for f^{est}_{nonBC}.

2.4. Attribution of Light Absorption to BC, OC, and Iron

[22] Calculation of C^{est}_{BC} and f^{est}_{nonBC} requires attribution of total measured absorption to BC and non-BC constituents. As noted above, local soil appears to be mixed in with surface snow across much of north China. In addition, large desert areas in the region are likely a significant source of MD to north China snow. Iron is the primary light-absorbing constituent in MD, with the spectral absorption characteristics of the dust dependent on the form of the iron oxide [*Sokolik and Toon*, 1999; *Lafon et al.*, 2004, 2006]. Over northern China, MD iron is most often found in the form of goethite [*Ji et al.*, 2002; *Lafon et al.*, 2006; *Mao et al.*, 2010], so all iron in our samples is assumed to be in this form. Soil also contains light-absorbing organics in the form of HULIS. Combustion sources that emit BC will also emit light-absorbing organic constituents, or "brown carbon" [*Andreae and Gelencsér*, 2006], and these will be deposited to snow along with BC.

[23] We therefore attribute light absorption to three sources: BC, iron (Fe), and OC, where OC is a mixture of soil organics and combustion brown carbon. Absorption, measured as an optical depth (τ_{tot}) on the sample filters, can be expressed as shown by equation (2):

$$\tau_{tot}(\lambda) = \beta_{BC}(\lambda)\cdot L_{BC} + \beta_{OC}(\lambda)\cdot L_{OC} + \beta_{Fe}(\lambda)\cdot L_{Fe} \quad (2)$$

where β is the MAE (in $m^2\ g^{-1}$) of a given constituent and L is that constituent's loading ($g\ m^{-2}$) on the filter. L_{Fe} is known from the chemical analysis. β_{BC}, β_{OC}, and β_{Fe} are assumed to be 6.3, 0.3, and 0.9 $m^2\ g^{-1}$, respectively, at 550 nm, and absorption Ångström exponents for BC, OC, and Fe of 1.1, 6, and 3 are used to determine β as a function of wavelength. Using the measured value of τ_{tot} at two wavelengths (450 and 600 nm), equation (2) can be solved for the two unknowns: L_{BC} and L_{OC}. L_{BC} is converted to a concentration, C^{est}_{BC}, based on the exposed area of the filter and the volume of filtered snow meltwater. Spectrally resolved absorption optical depth due to BC and non-BC (Fe + OC) are weighted by the down-welling solar spectrum to calculate f^{est}_{nonBC}. Finally, the absorption Ångström exponents of non-BC constituents are calculated as a linear combination of contributions to light absorption by OC and Fe, that is, equation (3):

$$\mathring{A}_{non-BC} = FOC\mathring{A}_{OC} + FFE\mathring{A}_{Fe}. \quad (3)$$

[24] All absorption Ångström exponents presented herein apply to the same range of wavelengths (450–600 nm), and *FOC* and *FFE* refer to the fractional contributions to absorption in that spectral band by OC and Fe oxides.

[25] The measured value of $\mathring{A}$ for local soil samples can be compared to $\mathring{A}_{non\text{-}BC}$ for a given measurement site as an indicator of whether local soil might be dominating the non-BC absorption. Similarly, when $\mathring{A}_{non\text{-}BC}$ is close to that measured for the total particulates on our sample filters, $\mathring{A}_{tot}$, this indicates that snow impurity light absorption is dominated by non-BC constituents.

[26] The values of β_{BC} and $\mathring{A}_{BC}$ used in our analysis are based on Mie calculations of absorption using the size distribution and refractive index of the synthetic BC calibration standard used to convert measured absorption to BC mass. The value of 6.3 $m^2\ g^{-1}$ is 20% lower than the recommended value of 7.5 $m^2\ g^{-1}$ for freshly emitted BC [*Bond and Bergstrom*, 2006] and about 45% lower than the recommended value for aged (coated) BC [*Bond et al.*, 2006]. While BC deposited to north China snow is likely aged (i.e., has been in the atmosphere for 1 day or more), BC on our sample filters has likely been stripped of soluble coatings in the process of melting and filtering the snow sample. Thus, it is likely that β_{BC} of the BC on our sample filters is closer to that of fresh BC than of coated BC. The selected $\mathring{A}_{BC}$ of 1.1 is consistent with multiple measurements of $\mathring{A}$ for BC from combustion sources [*Rosen et al.*, 1978; *Bond et al.*, 1999; *Bond*, 2001; *Bergstrom et al.*, 2002, 2007; *Kirchstetter et al.*, 2004; *Schnaiter et al.*, 2003, 2005; *Clarke et al.*, 2007; *Adachi and Buseck*, 2008].

[27] As noted earlier, Fe is assumed to be associated with goethite, and the selected values of β_{Fe} (0.9 $m^2\ g^{-1}$) reflects this [*Bedidi and Cervelle*, 1993]. If all of the Fe oxide was instead in the form of hematite, β_{Fe} would be about 50% higher [*Bedidi and Cervelle*, 1993] and the derived loading (L_{Fe}) consequently about 50% lower. The value of $\mathring{A}_{Fe}$ we use is based on optical measurements of amibent MDs from China and elsewhere. Measured values typically range from

~2 to 4 from a broad range of sites [*Yang et al*., 2009, *Fialho et al*., 2006], justifying our selection of 3. The selection of appropriate values of β_{OC} and $\AA_{OC}$ are more difficult, because the light-absorbing OC can be a variable mix of soil organics and combustion brown carbon. The optical properties of brown carbon vary with burn material and burn temperature [*Bond et al*., 1999; *Bond*, 2001] and those of soil organics vary with composition and therefore source location. There was no basis for assigning a variable OC composition, so we used fixed values of $\beta_{OC} = 0.3\ m^2\ g^{-1}$ [*Yang et al*., 2009] and $\AA_{OC} = 6$, the latter of which is intermediate to the value of 5 used for combustion organics by *Doherty et al*. [2010] in analyzing Arctic snow samples and the higher values of $\AA$ (~6–7) expected for HULIS in soils [*Hoffer et al*., 2006]. However, these assumed values of β_{OC} and $\AA_{OC}$ are both highly uncertain, and this uncertainty is propagated to uncertainty in C_{BC}^{est}, f_{nonBC}^{est} and the apportioning of light absorption to BC, OC, and Fe oxides.

[28] Use of absorption Ångström exponents to separate contributions to absorption by BC (section 2.3) and by OC and Fe (equation (3)) is appropriate to the degree that our samples' particulate absorption actually varies linearly with wavelength in log/log space. To test the degree to which this is the case, we compared the spectrally resolved optical depth as given using the derived values of *FBC*, *FOC*, and *FFE* at 450 nm then extrapolating to all other wavelengths using our assumed values for $\AA_{BC}$, $\AA_{OC}$, and $\AA_{Fe}$ to the spectrally resolved optical depth as measured with the ISSW spectrophotometer. We found that the two typically agreed to within 5%, except at the very shortest (<410 nm) and longest (>700 nm) wavelengths, where the two could diverge by up to 15–20%.

[29] As a very conservative estimate of uncertainty in C_{BC}^{est} and f_{nonBC}^{est} due to uncertainty in our assumed absorption Ångström exponents for BC and non-BC constituents, we allow $\AA_{BC}$ to range from 0.8 to 1.9, and we allow $\AA$ of the non-BC constituents to vary from $\AA_{non\text{-}BC}$ −1.5 to $\AA_{non\text{-}BC}$ +2.0, where $\AA_{non\text{-}BC}$ varies from sample to sample (Table 1), depending on the estimated contributions to non-BC absorption by OC and Fe. This range for $\AA_{BC}$ spans its theoretically possible lower and upper bounds [*Lack and Cappa*, 2010]. The resulting lower and upper bounds on C_{BC}^{est} and f_{nonBC}^{est} are reported along with our central estimates for these parameters. Values of $C_{BC}^{est} < 0$ and $f_{nonBC}^{est} > 100$ are clearly not physically possible and indicate where these uncertainty bounds exceed the true possible bounds in $\AA_{non\text{-}BC}$ and $\AA_{non\text{-}BC}$ for that sample.

[30] A recent analysis by *Schwarz et al*. [2012] highlights the uncertainty in the attribution of light absorption in the ISSW measurements. That study compared measurements of BC concentrations with the ISSW versus with a single-particle soot photometer (SP2) instrument for water samples containing gravimetrically determined concentrations of synthetic BC (fullerene), a dust standard, polystyrene latex spheres (PSLs), a fullerene/dust mixture, or a fullerene/PSL mixture. In these samples, the only non-BC absorber is the dust standard. Using measurements of solutions containing only dust, the non-BC absorption Ångström exponent could be perfectly determined with the ISSW. Nominally, this should allow for highly certain determination of C_{BC}^{est} in mixtures of BC (fullerene) and the dust standard. However, *Schwarz et al*. [2012] report up to a factor of 3 high bias in C_{BC}^{est} from the ISSW for the fullerene/dust mixtures. In addition, the instrument responded to solutions of nonabsorbing PSLs. In contrast, the ISSW was able to accurately measure a range of concentrations of pure BC. This indicates that the ISSW responds to particulate scattering, not just absorption, in contrast to earlier tests showing an insensitivity to variations in sample scattering [*Doherty et al*., 2010; *Grenfell et al*., 2011]. The value of C_{BC}^{est} reported here may therefore have a significant high bias, and f_{nonBC}^{est} a low bias, especially for samples containing large concentrations of dust or local soil.

2.5. Optical Analysis of Local Soil Samples

[31] As noted above, it was visually apparent during field sampling that local soil was often mixed with the snow and contributed to surface snow particulate light absorption. The procedure discussed above uses assumed optical properties for BC and non-BC absorbers to attribute particulate light absorption in snow samples to BC, OC, and Fe. However, it does not quantify the contribution specifically of local soil to total particulate light absorption in the snow. The absorption Ångström exponents for the non-BC constituents, especially OC, are very uncertain, so attribution to BC, OC, and Fe is correspondingly very uncertain, especially for samples with high $\AA_{tot}$ [i.e., *Doherty et al*., 2010, Figure 16]. Even if light absorption is accurately apportioned to BC, OC, and Fe, this analysis cannot say whether the OC is from combustion aerosol or from soil organics, or whether the Fe and soil organics are of local origin or were deposited after long-range transport (e.g., MD from deserts). Therefore, an additional step was taken to understand the role of local soils in snowpack particulate light absorption. At many of the sites, soil samples were collected for analysis of their light-absorbing properties, specifically their absorption Ångström exponent ($\AA_{soil}$). If $\AA_{tot}$ from the snow samples is very similar to $\AA_{soil}$, then the local soil is probably playing a dominant role in snow particulate light absorption. Qualitatively, this same comparison can be made by visually inspecting the color of filters from snow samples against filters loaded with local soil (Figure 5). It can be seen that particles in the snow are always somewhat more gray (less brown or orange) than the soil samples (top row of Figure 5 vs. bottom row of Figure 5), but there are regional differences in both the soil color and in the degree to which local soil contributes to snow total particulate light absorption. In snow/soil sample pairs from the Mongolian grasslands (site 3 in region 2; left two filters in Figure 5) and from region 1, where the snow was very thin (site 45 in region 1; right two filters in Figure 5), the colors of the soil and snow particulate samples are similar, indicating the local soil contributes significantly to snow particulate light absorption. In northeast China, where the snowpack is deeper and the sample sites closer to industrial pollution sources (site 22 in region 3; middle two filters in Figure 5), the particles in the snow are almost completely gray and the soil itself is brown.

[32] Soil samples were collected from 26 out of the 46 sites. In the lab, these were mixed with Milli-Q water in a cleaned glass beaker and sonicated for approximately 10 minutes to break up large conglomerates of soil. The

Table 1. Results Using the Average Values of the Left and Right Settled Snow Samples and Local Soil Samples During the 2010 China Field Campaign[a]

Site	Layer	Latitude N	Longitude E	Site Average Snow Depth (cm)	Sample Depth (cm)		C_{BC}^{equiv}	$C_{BC}^{\max}$	C_{BC}^{est}	f_{nonBC}^{est}	$R_{stir,settle}$	$\mathring{A}_{tot}$	$\mathring{A}_{soil}$
					Top	Bottom	(ng/g)	(ng/g)	(ng/g)	(%)		450:600 nm	450:600 nm
Region 1. Qilian Mountains													
41	1	36°26′	101°04′	2	0	3	2954	—	—	—	2.8	3.76	3.01
	2				3	7	2079	—	—	—	2.3	3.49	
42	1	36°17′	101°53′	2	0	2	1438	—	—	—	1.6	3.77	3.22
	2				2	6	1203	—	—	—	1.4	3.93	
	3				6	10	1081	—	—	—	1.8	4.01	
43	1	37°39′	100°27′	10	0	5	3042	—	—	—	1.8	4.11	4.34
	2				6	8	421	—	—	—	1.8	3.67	
	3				9	15							
	4				15	20	1533	—	—	—	1.9	3.65	
44	1	38°00′	100°13′	15	0	2	426	—	—	—	1.5	3.55	3.56
	2				2	6	588	—	—	—	1.7	3.50	
45	1	38°11′	100°55′	5	0	2	563	—	—	—	1.2	3.69	3.79
	2				3	7	5580	—	—	—	—	4.49	
46	1	38°36′	99°34′	4	0	1	650	—	—	—	2.2	3.97	3.24
	2				0	4	810	—	—	—	1.9	4.03	
	3				2	6	5285	—	—	—	—	5.68	
	4				6	12	1378	—	—	—	1.5	3.90	
	5				12	15	3391	—	—	—	1.9	4.36	
	6				15	25	3531	—	—	—	1.5	4.27	
	7				25	27	2408	—	—	—	2.2	4.27	
	8				27	35	831	—	—	—	—	3.72	
Region 2. Inner Mongolia													
1	1	41°18′	107°04′	5	0	3	821	—	—	—	3.4	4.19	5.56
	2				3	8	6343	—	—	—	—	6.18	
2	1	41°41′	106°59′	5	0	4	920	—	—	—	2.3	4.89	5.63
	2				10	15	1052	—	—	—	5.8	4.68	
	3				15	20	12,194	—	—	—	—	6.22	
3	1	41°51′	108°02′	3	0	5	1048	448	300 (74, 502)	71 (52, 92)	4.2	4.12	6.24
	2				5	10	1180	544	398 (159, 618)	67 (49, 88)	2.8	3.90	
4	1	40°48′	110°04′	12	0	3	1357	994	864 (621, 1108)	36 (18, 53)	—	2.11	
5	1	41°36′	109°55′	4	0	5	1634	945	801 (516, 1084)	50 (33, 67)	—	2.97	4.46
6	1	41°23′	110°36′	7	0	5	1163	676	567 (370, 765)	51 (34, 68)	3.3	3.00	4.71
	2				5	10	2760	1177	764 (177, 1289)	72 (53, 93)	5.0	4.11	
7	1	41°34′	111°44′	5	3	6	4099	—	—	—	—	4.85	
	2				10	20	865	401	290 (78, 317)	67 (48, 87)	3.9	3.82	
8	3	43°42′	112°29′		20	30	266	119	82 (26, 132)	69 (50, 90)	2.0	3.93	5.37
9	1	43°42′	112°29′	10	0	4	420	198	131 (34, 216)	69 (48, 92)	2.6	3.76	
	2				4	8	460	217	146 (40, 238)	68 (48, 91)	1.4	3.72	
	3				8	12	208	92	57 (9, 99)	72 (52, 96)	—	3.92	
10	1	43°54′	114°24′	7	0	4	398	178	98 (–2, 182)	74 (53, 99)	1.7	3.89	
11	1	43°20′	116°22′	6	0	5	466	229	170 (72, 260)	63 (44, 85)	—	3.54	
	2				5	10	311	147	107 (41, 166)	66 (47, 87)	2.9	3.64	
	3				10	15	545	271	204	63	—	3.53	
12	1	44°14′	116°30′		0	5	2543	1050	641 (74, 1136)	75 (55, 97)	—	4.20	

					Top	Bottom	(ng/g)	(ng/g)	(ng/g)	(%)		450:600 nm	450:600 nm
13	1	43°54′	115°18′	1	3	8	1445	624	413 (79, 704)	71 (51, 95)	—	3.98	
14	1	44°34′	115°51′	5	0	3	12,980	5368	3705 (836, 6259)	72 (53, 94)	—	4.15	4.46
	2				4	10	2003	860	615 (184, 1003)	69 (50, 91)	4.7	3.98	
15	1	45°40′	117°42′	7	0	3	683	365	286 (141, 419)	58 (39, 79)	2.5	3.24	
	2				3	8	392	216	172 (91, 247)	56 (37, 77)	—	3.14	
16	1	46°20′	121°55′	3	0	2	1522	888	756 (462, 1038)	50 (32, 70)	—	2.90	
	2				4	7	2467	1296	1024 (503, 1500)	59 (39, 79)	—	3.26	
17	1	47°35′	119°21′	18	0	6	509	345	290 (180, 391)	43 (23, 65)	1.6	2.37	
	2				6	12	279	202	176 (120, 229)	37 (18, 57)	2.4	2.15	
	3				12	18	1270	873	742 (471, 993)	42 (22, 63)	—	2.32	
18	1	48°22′	117°39′	4	0	3	655	412	345 (221, 465)	47 (29, 66)	3.1	2.66	3.11
	2				3	8	927	588	495 (320, 665)	47 (28, 65)	2.1	2.64	
	3				8	12	742	468	394 (255, 528)	47 (29, 66)	2.2	2.63	
19	1	49°33′	118°32′	10	0	4	551	392	326 (192, 443)	41 (20, 65)	1.3	2.20	2.53
	2				4	9	593	433	366 (228, 489)	38 (18, 62)	1.4	2.11	
	3				9	14	664	486	409 (251, 549)	38 (17, 62)	1.2	2.14	
Region 3. Northeast Border													
20	1	50°34′	121°02′	20	0	3	374	326	295 (231, 326)	21 (3, 39)	—	1.52	
	2				3	7	439	250	137 (–24, 253)	69 (43, 105)	—	3.18	
	3				7	11	248	187	153 (90, 206)	39 (17, 64)	—	2.09	
	4				11	15	187	146	124 (81, 162)	34 (13, 57)	—	1.93	
21	1	50°19	124°43′	18	0	4	140	123	112 (88, 137)	20 (2, 37)	—	1.44	3.04
	2				4	8	104	82	70 (47, 91)	33 (13, 55)	—	1.84	
	3				8	12	133	103	88 (57, 115)	34 (13, 57)	—	1.90	
22	1	51°04′	126°27′	21	0	3	100	78	68 (50, 86)	32 (14, 50)	—	1.91	2.81
	2				3	7	80	63	56 (42, 70)	31 (13, 48)	—	1.85	
	3				7	11	87	68	60 (45, 76)	31 (13, 48)	—	1.87	
	4				11	15	63	48	41 (30, 53)	34 (16, 53)	—	1.99	
23	1	51°02′	126°56′	15	0	2	118	93	79 (53, 103)	33 (13, 55)	—	1.85	
	2				2	6	82	63	52 (33, 69)	36 (15, 60)	—	1.95	
	3				7	11	99	79	68 (46, 88)	32 (12, 54)	—	1.83	
24	1	50°19′	120°14′	25	0	1	203	148	121 (77, 162)	40 (21, 62)	—	2.19	
	2				1	5	121	89	72 (46, 96)	40 (21, 62)	—	2.18	
	3				5	9	101	81	71 (52, 90)	30 (12, 48)	—	1.83	
	4				9	13	524	433	396 (301, 494)	25 (6, 43)	—	1.74	
	5				13	18	121	98	88 (67, 110)	27 (9, 44)	—	1.73	
Region 4. Northeast Industrial													
25	1	49°41′	127°28′	30	2	6	618	486	415 (259, 550)	33 (11, 58)	—	1.93	3.69
	2				6	10	216	177	156 (110, 200)	28 (8, 49)	—	1.71	
	3				10	15	412	335	296 (203, 381)	28 (7, 51)	—	1.75	
	4				15	20	256	212	190 (136, 241)	26 (6, 47)	—	1.66	
26	1	49°15′	129°17′	25	0	2	1497	996	867 (572, 1152)	41 (23, 61)	—	2.44	
	2				2	6	204	157	141 (109, 175)	32 (15, 47)	—	1.98	
	3				6	11	272	215	196 (156, 241)	28 (11, 43)	—	1.85	
	4				11	16	106	83	74 (58, 92)	30 (14, 45)	—	1.91	

(*Continues*)

Table 1. (Continued)

Site	Layer	Latitude N	Longitude E	Site Average Snow Depth (cm)	Sample Depth (cm)		C_{BC}^{equiv}	$C_{BC}^{\max}$	C_{BC}^{est}	f_{nonBC}^{est}	$R_{stir,settle}$	$\mathring{A}_{tot}$	$\mathring{A}_{soil}$
					Top	Bottom	(ng/g)	(ng/g)	(ng/g)	(%)		450:600 nm	450:600 nm
	5				16	20	114	90	82 (65, 100)	28 (12, 42)	—	1.81	
27	1	48°30′	130°35′	40	0	4	988	718	615 (399, 814)	38 (18, 60)	—	2.16	3.18
	2				4	9	303	258	240 (192, 292)	21 (4, 37)	—	1.56	
	3				9	15	174	138	122 (91, 153)	30 (12, 48)	—	1.81	
	4				15	21	217	171	150 (109, 191)	31 (12, 50)	—	1.88	
	5				21	27	119	92	80 (57, 102)	33 (14, 52)	—	1.91	
28	1	47°33′	130°36′	35	0	5	1898	1561	1435 (1149, 1752)	24 (8, 39)	1.3	1.63	3.66
	2				5	15	374	307	279 (219, 344)	25 (8, 41)	—	1.72	
	3				15	25	254	205	185 (144, 229)	28 (10, 44)	1.3	1.78	
29	1	46°32′	129°51′		0	1.5	2804	2344	2208 (1862, 2634)	21 (6, 34)	3.0	1.62	4.25
	2			12	2	6	1246	1089	1029 (889, 1211)	17 (3, 29)	1.6	1.46	
	3				6	10	785	697	664 (577, 779)	15 (1, 26)	1.2	1.42	
30	1	46°37′	125°30′	12	0	1	3365	2783	2611 (2156, 3148)	22 (6, 36)	1.7	1.69	3.69
	2				1	6	865	703	648 (528, 786)	25 (9, 39)	1.3	1.76	
31	1	47°45′	126°12′	17	0	1	1304	1154	1066 (811, 1319)	19 (0, 39)	1.1	1.44	
	2				1	6	236	208	183 (137, 228)	22 (3, 42)	1.4	1.47	
	3				6	9	1588	1374	1251 (907, 1576)	21 (1, 43)	1.4	1.54	
32	1	47°30′	123°33′	4	0	1	1806	1471	1344 (1040, 1667)	26 (8, 42)	0.7	1.77	
	3				5	6	1143	849	743 (524, 958)	35 (16, 54)	2.0	2.07	
	4				6	9	464	366	327 (247, 410)	29 (12, 47)	1.2	1.86	
33	1	43°48′	130°58′	30	0	3	1621	1266	1149 (900, 1420)	29 (12, 44)	1.1	1.85	
	2				3	7	560	477	446 (375, 532)	20 (5, 33)	1.1	1.50	
	3				7	11	199	170	157 (132, 188)	21 (6, 34)	0.9	1.51	
	4				11	15	101	90	84 (72, 99)	17 (2, 29)	1.0	1.40	
	5				15	20	314	286	272 (236, 319)	13 (–2, 25)	1.3	1.31	
34	1	43°50′	128°54′	8	0	2	2377	1650	1329 (710, 1852)	44 (22, 70)	1.4	2.32	
	2				2	5	2218	1563	1288 (727, 1771)	42 (20, 67)	1.4	2.24	
	3				5	8	2366	1718	1462 (887, 1969)	38 (17, 62)	—	2.14	
	4				8	11	2545	1817	1539 (913, 2086)	39 (18, 64)	—	2.17	
	5				11	15	2861	2124	1843 (1177, 2441)	36 (15, 59)	—	2.05	
35	1	44°42′	127°35′	21	0	2	2378	1758	1628 (1297, 2004)	31 (16, 45)	1.6	2.09	
	2				2	5	2164	1777	1675 (1423, 1991)	23 (8, 34)	—	1.70	
	3				5	8	1151	853	783 (620, 965)	32 (16, 46)	1.2	2.11	
	4				8	11	1015	792	747 (618, 902)	26 (11, 39)	1.7	1.87	
	5				11	15	940	799	762 (657, 898)	19 (4, 30)	1.5	1.59	
36	1	45°09′	124°27′	5	0	4	769	612	542 (393, 688)	30 (11, 49)	1.7	1.79	
	2				1	3	2327	1957	1803 (1366, 2250)	23 (3, 41)	1.2	1.66	
37	1	43°23′	126°30′	15	0	3	1674	1165	1027 (720, 1334)	39 (20, 57)	1.1	2.32	4.24
	2				3	5	4758	2997	2510 (1546, 3419)	47 (28, 67)	—	2.66	
	3				5	10	919	665	585 (427, 747)	36 (19, 53)	—	2.20	
	4				10	15	1025	671	554 (353, 754)	46 (27, 65)	1.8	2.58	
	5				15	20	952	657	562 (387, 735)	41 (23, 59)	1.8	2.38	
38	1	42°29′	126°47′	23	0	3	3567	2372	2139 (1519, 2775)	39 (21, 56)	—	2.44	2.63
	2				3	6	3088	2282	2100 (1634, 2613)	32 (15, 47)	1.4	2.14	
	3				6	10	3294	2063	1747 (1138, 2347)	47 (29, 65)	1.6	2.77	
	4				10	15	1255	919	846 (650, 1059)	33 (16, 48)	2.1	2.20	

(*Continues*)

39	1	42°00′	127°33′	32	0	2	1699	1237	1130 (880, 1405)	33 (17, 48)	1.3	2.15	3.59
	2				3	5	1873	1320	1212(920, 1526)	35 (19, 51)	1.5	2.28	
	3				6	10	749	592	545 (447, 661)	27 (12, 40)	1.1	1.88	
	4				10	15	1180	864	797 (624, 988)	32 (16, 47)	1.3	2.12	
	5				15	20	341	266	246 (202, 298)	28 (13, 41)	1.3	1.88	
40	1	41°43′	125°11′	23	0	1	1576	1153	1025 (744, 1311)	33 (16, 50)	—	2.11	3.04
	2				2	4	2348	1722	1530 (1093, 1966)	35 (16, 53)	1.6	2.13	
	3				4	6	2830	2146	1927 (1426, 2440)	32 (14, 49)	1.2	2.02	
	4				6	12	2544	1598	1263 (676, 1786)	51 (30, 74)	1.1	2.75	
	5				12	18	1359	1052	955 (728, 1195)	30 (12, 47)	1.7	1.93	

[a]For C_{BC}^{est} and f_{nonBC}^{est}, ranges about the central estimate are given in parenthesis, where the ranges reflect a very conservative estimate of uncertainty in the apportionment of absorption to BC and non-BC constituents (section 2.4).

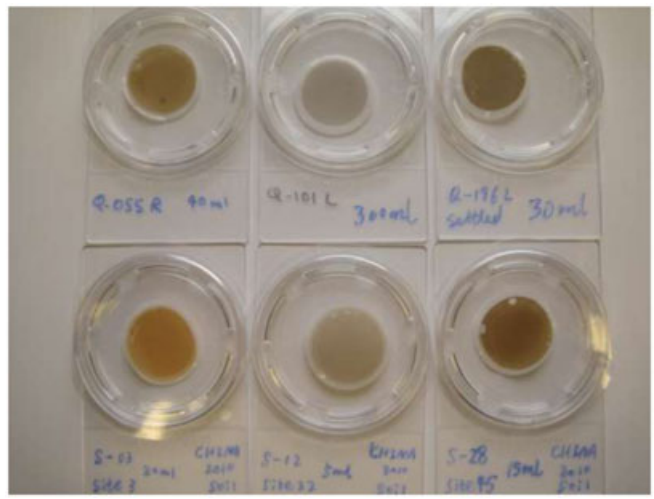

Figure 5. Examples of filters of snow samples (top row) and soil samples (bottom row) from sites 3, 22, and 45.

soil/water solution was then allowed to sit for 3 ~ 5 minutes so that very large particles could settle in the beaker. The supernatant fluid was then filtered through 0.4 μm Nuclepore filters, using the same procedure used to filter the melted snow samples. These filters were optically analyzed with the ISSW spectrophotometer to determine the soil absorption Ångström exponent, $\mathring{A}_{soil}$, which, like $\mathring{A}_{tot}$, is defined for the 450–600 nm wavelength range.

2.6. Comparison With Modeled Snow BC Concentrations

[33] Measured concentrations of BC in surface snow (C_{BC}^{est}) are compared to concentrations simulated with the National Center for Atmospheric Research (NCAR) Community Atmosphere Model (CAM 3.1). The model values correspond to those in surface snow from the study described in detail by *Flanner et al*. [2009]. Observations are paired with model values, which are calculated as the average of the monthly model values from January and February for the grid box that contains the sample site. Model BC and OC were treated prognostically using FF and biofuel emissions corresponding to the year 1996, as given by *Bond et al*. [2004], and open burning emissions are for the year 2002 (GFED version 2) [*van der Werf et al*., 2006]. Year 2002 open burning emissions were used because this is considered a "typical" BB year. Thus, the modeled and observed values do not correspond in terms of the year of emissions. Interannual differences in the transport and deposition rates of atmospheric light-absorbing aerosol also are not accounted for in this comparison. However, the observational data set is sufficiently geographically broad that this comparison is useful for testing whether observed and modeled surface snow BC distributions are similar in magnitude and follow the same general spatial patterns.

3. Results

[34] Over 400 snow samples were collected from 46 sites in the 2010 north China field campaign. Values of C_{BC}^{est}, $C_{BC}^{\max}$, C_{BC}^{equiv}, f_{nonBC}^{est}, $\mathring{A}_{tot}$, and $\mathring{A}_{soil}$ are given in Table 1 for each measurement site at each depth where snow was sampled. The reported values are for the settled samples, which do

Table 2. Surface and Subsurface Snow Sample Median Values Within the Four Sample Regions Shown in Figure 1

Regions	Layers		C_{BC}^{equiv} (ng/g)	C_{BC}^{est} (ng/g)	f_{nonBC}^{est} (%)	$\AA_{tot}$ 450:600 nm
Snow samples						
1. Qilian	Surface	Average	1550	n/a	~100	3.9
Mountains	Subsurface	Average	2250		~100	4.1
2.Inner Mongolia	Surface	Median	820 ± 3060	340 ± 910	55 ± 15	3.6 ± 0.8
	Subsurface	Median	900 ± 2730	380 ± 270	60 ± 15	3.6 ± 0.8
3. Northeast	Surface	Average	190	135	30	1.8
border	Subsurface	Average	170	105	40	2.0
4. Industrial	Surface	Median	1720 ± 840	1220 ± 600	30 ± 10	2.1 ± 0.3
Northeast	Subsurface	Median	900 ± 1060	615 ± 640	30 ± 10	1.9 ± 0.3

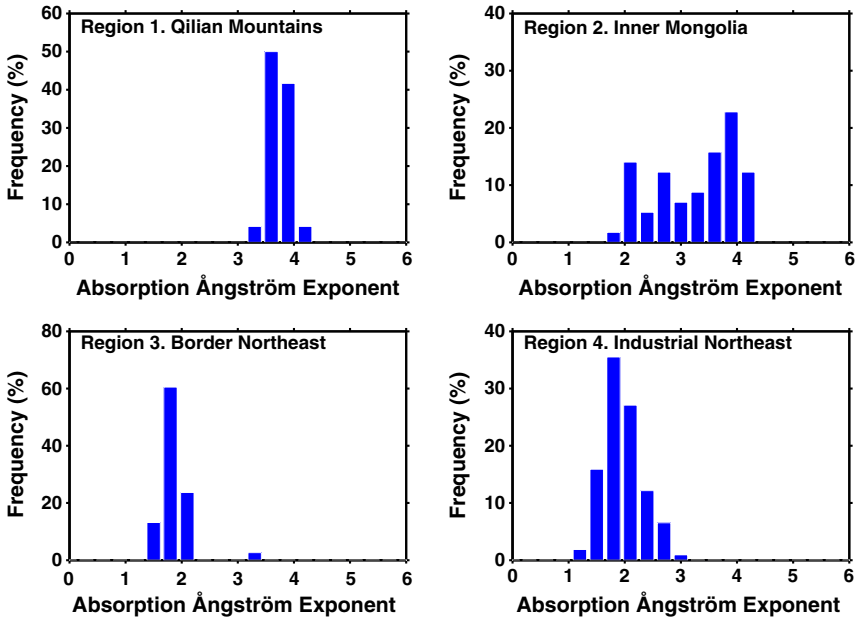

Figure 6. Histograms of the frequency of $\AA_{tot}$ (450–600 nm) for snow samples in each of the four regions. Samples from all snow depths are included.

not include very coarse-grained particles. We therefore also report on $R_{stir,settle}$, which indicates how much spectrally integrated solar absorption in the ambient snow is due to these large particles; that is, a value of $R_{stir,settle} = 2$ means the value of C_{BC}^{est} reported in Table 1 should be doubled in order to accurately represent absorption by all snow particles. Thus, $R_{stir,settle}$ provides a first-order estimate of the contribution of local soil to total snow particulate light absorption.

[35] The data in Table 1 are separated into four regions (as shown in Figure 1): the Qilian Mountains (sites 41–46), Inner Mongolia (sites 1–19), the Northeast Border (sites 20–24), and the Northeast Industrial area (sites 25–40). Table 2 presents regional values for the surface snow layer and for all subsurface layers as a single group. For regions 1 and 3, with less than six sites in each region, the reported values are averages across the sites; for regions 3 and 4, which had a larger number of sites, the median values and standard deviations are also reported.

[36] Histograms of $\AA_{tot}$ by region are shown in Figure 6. The absorption Ångström exponent is driven primarily by the composition of the aerosol and secondarily by the aerosol size distribution. Therefore, variations in $\AA_{tot}$ reflect variations in the source of light-absorbing particulates in the snow. Pure BC could theoretically be as low as 0.8 or as high as 1.9 [*Lack and Cappa*, 2010], but measurements of BC from combustion sources indicate that it is typically close to 1.0 [*Rosen et al*., 1978; *Bond et al*., 1999; *Bond*, 2001; *Bergstrom et al*., 2002, 2007; *Kirchstetter et al*., 2004; *Schnaiter et al*., 2003, 2005; *Clarke et al*., 2007]. When combined with other light-absorbing constituents, the total aerosol from combustion sources has absorption Ångström exponents higher than that of pure BC, because the brown carbon coemitted with BC has a stronger wavelength dependence. Urban and industrial FF emissions typically have absorption Ångström exponents of 1.0–1.5 [*Millikan*, 1961; *Rosen et al*., 1978; *Bergstrom et al*., 2007]; BB aerosol absorption Ångströms tend to be higher, mostly falling in the range of 1.5–2.5 [*Kirchstetter et al*., 2004; *Bergstrom et al*., 2007]. However, FF emissions, such as from dirty coal, can have values comparable to that of BB aerosol [*Bond et al*., 1999; *Bond*, 2001], so $\AA_{tot}$ is not a

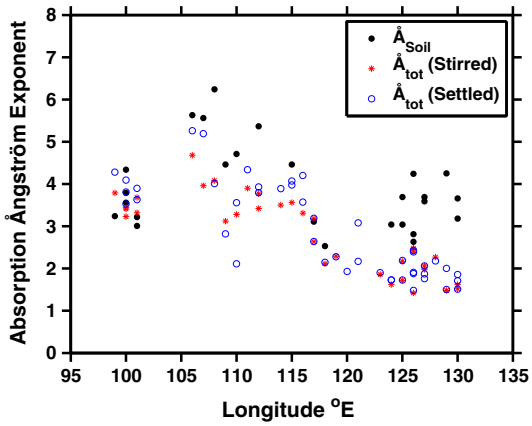

Figure 7. Particulate absorption Ångström exponents for snow ($Å_{tot}$) and soil ($Å_{soil}$) samples as a function of longitude, as measured with the ISSW spectrophotometer. Stirred samples have been agitated, so all but the very largest particles are captured by the filtration process. For settled samples, the snowmelt was left to sit for approximately 3–5 minutes after melting so the larger particles could settle to the bottom of the glass beaker.

definitive indicator of source. Generally, the absorption Ångström exponent of MD falls in the range of 2–5 [*Fialho et al.*, 2005; *Lafon et al.*, 2006; *Meloni et al.*, 2006; *Müller et al.*, 2009]. All of these sources of light-absorbing aerosol (FF combustion, biomass/biofuel combustion, and MD from nearby deserts) are expected to contribute to snow particulate light absorption in north China. In addition, local soil—which itself may contain BC and MD that has been deposited to the surface—is expected to contribute, and we have a direct measure of the site-specific absorption Ångström exponent for this source.

[37] At some sites, the absorption Ångström exponent of the snow particulates, $Å_{tot}$, was nearly equal to that of the local soil ($Å_{soil}$) (Figure 7); in other words, the soil and snow particulates were the same color. For these snow samples, it is likely that light absorption in the snowpack is dominated by the influence of local soil, which is mixed with the snow during wind events. This will be particularly likely to happen when the snow is thin and patchy, as was the case for all sites of region 1 and many sites in region 2. For these samples, it is not possible to state with confidence that any of the light absorption in the snow is due to BC. For sites 41–46 (Qilian Mountains), it was generally the case that $|Å_{soil}-Å_{tot}| < 1.0$, so for these sites we do not report values of C_{BC}^{est}, $C_{BC}^{\max}$, or f_{nonBC}^{est}. A value of C_{BC}^{equiv} is given for these sites as a metric for how much BC would need to be present to account for spectrally averaged solar absorption of 300–750 nm by all particulate light absorbers, which, in this case, is likely local soil. It is not an indication of the amount of BC in the snow.

[38] Calculation of C_{BC}^{est} and f_{nonBC}^{est} becomes highly uncertain when $Å_{tot}$ approaches $Å_{nonBC}$ because absorption by BC is calculated as a small difference of two larger numbers [*Doherty et al.*, 2010]. This was the case for sites 1 and 2 in region 2, so for these sites we also do not report C_{BC}^{est}, $C_{BC}^{\max}$, or f_{nonBC}^{est} but, again, we do report C_{BC}^{equiv} as a metric for total particulate light absorption.

[39] The local soil absorption Ångström exponent, $Å_{soil}$, can also be compared to the non-BC absorption Ångström exponent, $Å_{non\text{-}BC}$ (equation (3)) which is calculated based on the Fe content and assumptions about the Fe oxide and OC absorption Ångström exponents. At most locations, the two values are quite different (Figure 8), with $Å_{non\text{-}BC}$ quite a bit higher than $Å_{soil}$. Above, we have asserted that almost all of the light absorption at sites 41–46 is from local soil. If this is correct and $Å_{non\text{-}BC}$ accurately reflects the spectral absorption properties of the dominant non-BC absorbers, we would expect $Å_{non\text{-}BC}$ and $Å_{soil}$ to be equal for these sites. The fact that they are not means either that the local soil is not the dominant non-BC absorber or that our assumptions about $Å_{OC}$ and $Å_{Fe}$ (and/or their role in determining $Å_{non\text{-}BC}$) are inaccurate. The latter is likely the case for the sites where $Å_{soil}$ and $Å_{tot}$ are nearly equal, but in general it is not possible to test for error in how well our calculated values of $Å_{non\text{-}BC}$ represent the true spectral absorption properties of the non-BC absorbers.

3.1. Results by Region

3.1.1. Qilian Mountains (Region 1)

[40] The Qilian Mountains are located at the northern boundary of the Tibetan Plateau. In February 2010, the sampled region had thin, patchy snow. As Figure 2f shows, the surface in the Qilian Mountains is sandy soil with very little vegetation. During windy periods, this soil can be lofted and deposited onto the snow. Also, snowfall in this

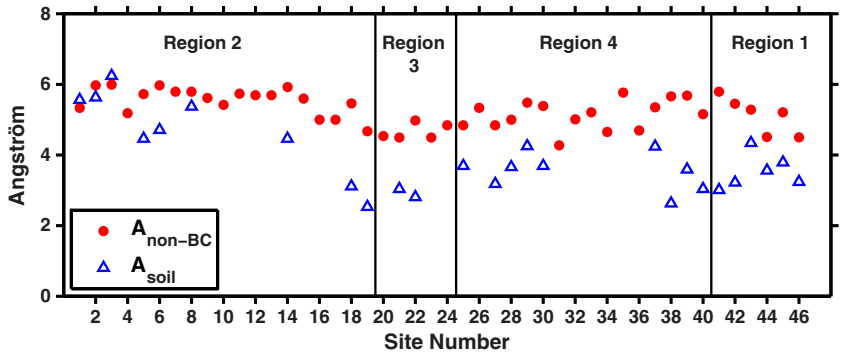

Figure 8. The absorption Ångström exponent for non-BC particulate constituents in the snow ($Å_{non\text{-}BC}$, red dots) and for local soil samples ($Å_{soil}$, blue triangles) as a function of site number (see Figure 1).

mountain range comes primarily in the spring when frontal systems entrain dust particles from disturbed and loose soils [*Wake and Mayewski*, 1994]. This is consistent with our finding that $\mathring{A}_{tot}$ and $\mathring{A}_{soil}$ are very similar (Figure 7)—that is, that most of the light-absorbing particulates in the snow in this region is due to local soil. As noted above, because of this we do not report values of C_{BC}^{est}, $C_{BC}^{\max}$, or f_{nonBC}^{est} for sites in this region. C_{BC}^{equiv} is reported, but we, again, emphasize that this is not a reflection of BC concentration, but rather a metric indicating the magnitude of total light absorption by all particulate matter in the snow.

[41] Figure 6 shows that $\mathring{A}_{tot}$ generally varied between ~3.5 and ~4.5 in this region. The narrowness of the absorption Ångström exponent distribution is indicative of a single dominant source of particulate light absorption, and as noted above the similarity of $\mathring{A}_{tot}$ and $\mathring{A}_{soil}$ in this region makes it likely this source is the local soil. Indeed, when very coarse-grained particles are also included in the sample, C_{BC}^{equiv} approximately doubles ($R_{stir,settle}$ in Table 1). High values of C_{BC}^{equiv} and $R_{stir,settle}$ point to the fact that not only is local soil probably the dominant absorber in the snowpack, but that it is present in high enough concentrations to significantly reduce the snow albedo. *Xu et al*. [2006] used a variation of the thermo-optical technique to quantify elemental carbon (EC) concentrations, which are the equivalent to our optically determined estimates of BC concentrations (C_{BC}^{est}) on the "1 July" glacier in the western Qilian Mountains, which is about 300 km west and 100–300 km north of our sites 41–46. They gathered several samples of newly fallen snow and found rather low EC concentrations of ~7 ng g^{-1} (range of 2–9 ng g^{-1} across four samples), and their finding of low EC concentrations is consistent with our conclusion that local soil dominates snow particulate light absorption in this region.

3.1.2. Inner Mongolia (Region 2)

[42] Snow cover in the grasslands of Inner Mongolia was more extensive than in the Qilian Mountains. Even though the snow cover was not as patchy, it was still thin (Table 1) and the region is quite windy [e.g., *Guo et al*., 2010, Figure 1a), so the snow was often wind blown and drifted. Snow samples were taken in a profile from the top of the snowpack down to the surface, with typical total snow depths of 4 ~ 10 cm. In most locations, such as sites 8 - (Figure 2b) and 14 (Figure 2c), the regional snow depth was only a few centimeters, so snow was usually collected from deep drifts.

[43] Most values of C_{BC}^{est} in this region fall within a range of ~100–600 ng g^{-1}, with a few lower values in the subsurface snow at sites 8 and 9, a few in the range 600–1200 ng g^{-1}, and one notably high concentration for the surface layer of site 14 with C_{BC}^{equiv} ~13,000 ng g^{-1} and C_{BC}^{est} ~3700 ng g^{-1}. This sample corresponds to the visibly dark surface layer shown in Figure 2c. Snow particulate $\mathring{A}_{tot}$ is 4.15, which is similar to the local soil absorption Angstrom, $\mathring{A}_{soil}$, of 4.46. $\mathring{A}_{nonBC}$ for this site is quite high (5.59), so a significant fraction of the total absorption is attributed to BC, leading to the high estimated BC concentration, C_{BC}^{est}. As noted in section 2.4, the selection of optical properties for, in particular, organics that are used to calculate $\mathring{A}_{nonBC}$ (equation (3)) are highly uncertain. A high bias in $\mathring{A}_{nonBC}$ corresponds to erroneously high values of C_{BC}^{est}, and that may be the case here, since both visual evidence and the similarity of $\mathring{A}_{tot}$ and $\mathring{A}_{soil}$ indicate that the large concentration of impurities in the site 14 surface layer are dominated by local soil. Comparison of the stirred and settled values of C_{BC}^{equiv} also indicate a significant role for very coarse-grained particles (i.e., of local origin) in snow light absorption in this region, with values of $R_{stir,settle}$ typically ~2–3, but very variable (range: 1.2–5.8).

[44] Region 2 (Figure 1) spans a broad range in longitude. There is no apparent trend in C_{BC}^{est} or C_{BC}^{equiv} (i.e., total particulate absorption optical depth) in moving from west to east; however, $\mathring{A}_{tot}$ and f_{nonBC}^{est} do have a longitudinal dependence. From 108°E to 117°E longitude (sites 3–14), $\mathring{A}_{tot}$ is quite consistently ~4 (3.9 ± 0.4; Table 1 and Figure 7) and f_{nonBC}^{est} is $68 \pm 6\%$ (Table 1), except at sites 4 and 5 where $\mathring{A}_{tot}$ is <3 and $f_{nonBC}^{est} < 50\%$. The lowest value of $\mathring{A}_{tot}$ in this region (2.1) is at site 4, consistent with its proximity to the industrial city of Baotou (40°32'N, 110°02'E). (This was the only site intentionally near a city.) The fact that $\mathring{A}_{tot}$ at site 5 is also lower than at other sites in the 108°E–117°E longitude range suggests that pollutants from Baotou may also be influencing snow particulate light absorption at this site, despite being >100 km north of the city. Moving northeast from 117°E to 120°E longitude, $\mathring{A}_{tot}$ decreases steadily from ~4 to ~2.0–2.5, and the fraction of absorption due to non-BC constituents decreases from ~70 to ~40%. Thus, BC shifts from being a secondary factor in total snowpack light absorption to the dominant absorber in moving from Inner Mongolia to northeast China.

3.1.3. Northeast Border (Region 3)

[45] The cleanest snow of the campaign was found in northeast China, along the border with Siberia (sites 20–24 in Figure 1). While there are some higher and lower concentrations, C_{BC}^{est} generally falls in the range 50–150 ng g^{-1}. The fraction of total particulate solar absorption due to non-BC (f_{nonBC}^{est}) is typically ~30–40%, so BC is the dominant absorber in this region. With the exception of one sample, $\mathring{A}_{tot}$ falls in the range 1.4–2.2, which is consistent with an FF combustion source. Thus, the non-BC absorption in this region is probably mostly or all from OC (brown carbon) coemitted with the BC from combustion sources. As shown below, $\mathring{A}_{tot}$ in this region is very similar to that found in the industrial area immediately to the south, indicating similar source types for the snow light-absorbing impurities in these two regions.

[46] Snow was somewhat deeper in this region than in Inner Mongolia, averaging 20 cm deep, but varying 18–25 cm, across the five sites sampled. Here and in the northeast industrial area (section 3.1.4), the snow was sufficiently deep that there was no need to preferentially sample from snow drifts, so the reported snow depths are representative.

3.1.4. Northeast Industrial Area (Region 4)

[47] Surface snow in this region had, on average, the highest BC concentrations of the four regions, especially south of 48ºN (sites 28–40), where C_{BC}^{est} for surface snow was typically ~1000–2000 ng g^{-1}. In addition, as for the northeast border sites, $\mathring{A}_{tot}$ was low (typically ~1.5–2.5; Figure 6) and most of the light absorption in the snowpack was attributable to BC (f_{nonBC}^{est} typically 15–45%). The soil from this region has an absorption Ångström exponent of ~2.7–4.5 (Figure 7) so it appears that, unlike in the Qilian Mountains

and parts of Inner Mongolia, local soil is not playing a large role in snowpack light absorption in this region or in region 3. Indeed, inclusion of very coarse-grained particles only increased C_{BC}^{equiv} by ~30% (see $R_{stir,settle}$ in Table 1) versus doubling it in regions 1 and 2. This makes sense, given that the snow at most sites in this region is ~15–20 cm deep and covers most of the land surface. In addition, eastern China has a higher concentration of industrial activities than do regions 1 and 2 [*Lu et al.*, 2011]. There is also less wind drifting because much of the land is forested, and we collected samples from open glades surrounded by trees.

3.2. Vertical Variations in Snowpack Light-Absorbing Particulates

[48] The snow in the Qilian Mountains (region 1) and Inner Mongolia (region 2) usually was not deep enough for vertical variations in snowpack impurities to be analyzed. For sites in these regions where there were samples from multiple depths, there is no apparent vertical variation in light-absorbing particulates concentrations or in $\mathring{A}_{tot}$ or f_{nonBC}^{est}. Some of this vertical homogeneity may be due to mixing during the drifting process. In the northeast (regions 3 and 4), particulate light absorption tends to be higher in the surface layer of snow than in the subsurface snow. In the northeast border region 3, the ratio of C_{BC}^{est} from the surface-most layer to the average of C_{BC}^{est} from all subsurface layers is 0.8 at one site (site 24), but for the other four sites it is greater than one (2.1, 1.4, 1.3, and 1.3). In the northeast industrial region, this ratio is greater than 1 for 12 of the 14 sites, and on average is 3 (range: 0.4–7.0). The low value of 0.4 is at site 40; the surface snow sample here was only 1 cm deep and was the only sample of newly falling snow from the whole campaign. This vertical variation in C_{BC}^{est} (also present for $C_{BC}^{\max}$ and C_{BC}^{equiv}) is not accompanied by vertical variations in $\mathring{A}_{tot}$, indicating that the source of the light-absorbing particles does not change with season. Thus, the higher surface concentrations must be due to an increase in aerosol deposition later in winter (February, when the snow was sampled) or to increased losses of surface snow water via sublimation later in the winter. A change in deposition could be through increased dry deposition and/or an increase in the mixing ratio of light-absorbing particulates to precipitation water content in falling snow. *Lu et al.* [2011] show that BC emissions in China peak in mid-winter (December/January) and fall off rapidly thereafter, but because wet deposition is determined by the mixing ratio of BC to snow water content, the two can not be directly related. The higher surface concentrations cannot be attributed to consolidation of BC and other particulates at the snow surface with melt because the temperatures at the sampled sites had not yet warmed enough for the snow to melt.

3.3. Light-Absorbing Particles in Stirred vs. Settled Samples

[49] As discussed in section 2.1, for all but the northeast border sites (20–27), filtrations were done of snow meltwater both immediately after stirring the meltwater and after letting the meltwater sit and settle for 3–5 minutes. This should be sufficient to allow particles >30 μm to settle from the top 10–15 cm of the water from which sample water was drawn. (The water was extracted from the beaker using a syringe whose orifice was just 1 cm below the water surface.) The intent was to separate the influence of impurities in the snowpack that were deposited after regional or long-range atmospheric transport from that of local soil mixed into the snow from surface wind or mechanical agitation from, for example, livestock. About one quarter of the stirred samples had filter loadings that were too high to measure with the ISSW and so are not included in this comparison. These will preferentially be high-concentration samples, so the role of

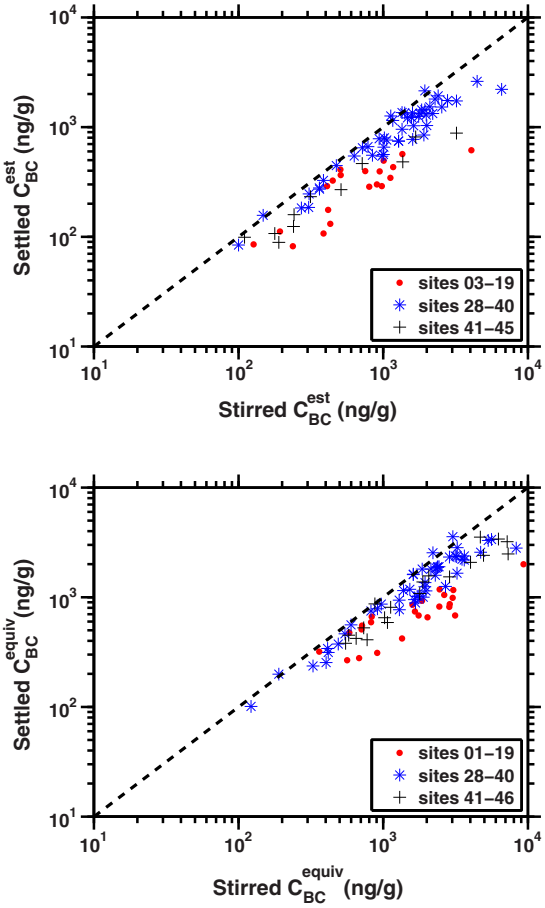

Figure 9. Stirred versus settled C_{BC}^{est} and C_{BC}^{equiv}. Sites 20–27 have only settled samples and so are not included in this figure.

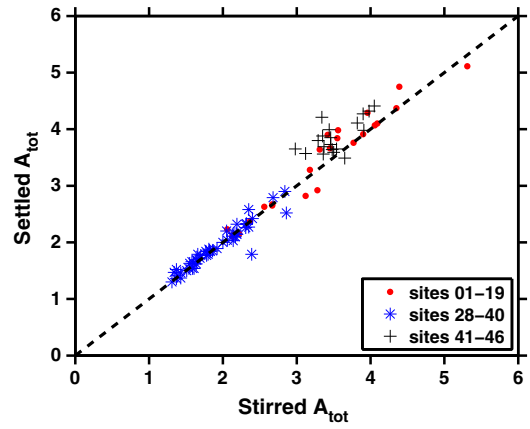

Figure 10. Measured values of $\mathring{A}_{tot}$ from stirred samples versus that from settled samples.

very coarse particles in lowering snow albedo is likely larger than is given by the difference shown here in C_{BC}^{equiv} for the stirred vs. settled samples.

[50] C_{BC}^{equiv} was, on average, a factor of 2 higher in the stirred vs. the settled samples, with a larger difference in regions 1 and 2 (factor of 2–3, on average) than in region 4 (factor of 1.5). This is consistent with our conclusion that local soil played a larger role in snowpack particulate light absorption in regions 1 and 2 than in regions 3 and 4. Ideally, letting large particles settle out of the snow meltwater would only remove non-BC constituents. If this were the case, C_{BC}^{equiv} would be lower in the settled samples than in the stirred samples, but C_{BC}^{est} would not change; instead, both C_{BC}^{est} and C_{BC}^{equiv} are lower for the settled vs. stirred samples (Figure 9). This could be the result of one or more of the following: First, it is possible that the local soil has BC attached to the coarse soil grains, so both are removed with settling. BC deposited to the snowpack separately from the soil might also become attached to the coarse-grained particles either in the snowpack or in the snow meltwater in the lab and again be removed with settling. Finally, it is possible that our calculated values of C_{BC}^{est} are, in fact, biased high because we have incorrectly attributed some of the light absorption due to coarse-grained particles (e.g., soil, dust) to BC, so that when the soil/dust is removed C_{BC}^{est} decreases.

[51] Comparison of $\mathring{A}_{tot}$ in the stirred vs. settled sample sets (Figure 10) provides some insight to the type of particulates that are excluded through letting the samples settle. For sites 28–40, in the northeast industrial region, $\mathring{A}_{tot}$ does not change with settling, so there does not appear to be a preferential loss of one type of light-absorbing particulates (e.g., soil vs. combustion particles). However, for the sites in region 1 (Qilian Mountains) and for some sites in region 2 (Inner Mongolia grasslands), $\mathring{A}_{tot}$ of the settled samples is higher than for the stirred samples. Because of the size of the particles removed through the settling process (>30 μm diameter), losses should be heavily weighted toward local soil or MD vs. combustion particles. Thus, higher values of $\mathring{A}_{tot}$ for settled vs. stirred samples would be consistent with two driving factors: First, the brown carbon in the combustion particles must have a higher absorption Ångström exponent than does the soil/dust. $\mathring{A}_{soil}$ varies ~2.5–4.5, though there are some higher values in the western grasslands of Inner Mongolia, where the soil is very orange. Absorption Ångström exponents of >5 for combustion organics are consistent with some studies [*Schnaiter et al*., 2006; *Shapiro et al*., 2009; *Chen and Bond*, 2010]. Second, the higher values of $\mathring{A}_{tot}$ in the settled samples imply that brown carbon must be having a significant influence on spectral light absorption in these samples.

[52] Finally, we remind the reader that all concentrations reported in Tables 1 and 2 are calculated from settled samples. As Figure 9 indicates, the actual amount of light absorption in the snowpack is about a factor of 2 higher when the influence of coarse-grained particles is included. This has direct implications for accurate representation of snow albedo reduction due to particulate impurities and resulting radiative forcing and climate warming.

3.4. Contributions to Particulate Light Absorption by BC, OC, and Fe

[53] As described in Section 2.4, the ISSW measurements of snow particulate absorption optical depth are combined with chemical analysis of Fe concentrations and assumptions about the mass absorption efficiencies and absorption Ångström exponents of BC, OC, and Fe oxide in order to attribute particulate light absorption to these three species. Inherent to this approach is an assumption that these three species are fully responsible for all particulate light absorption in our samples. Light-absorbing OC could comprise combustion aerosol (brown carbon), soil organics, and/or other biological organics (e.g., algae or broken-up pieces of plant material). BC and OC from combustion sources could be from FF burning, biofuel

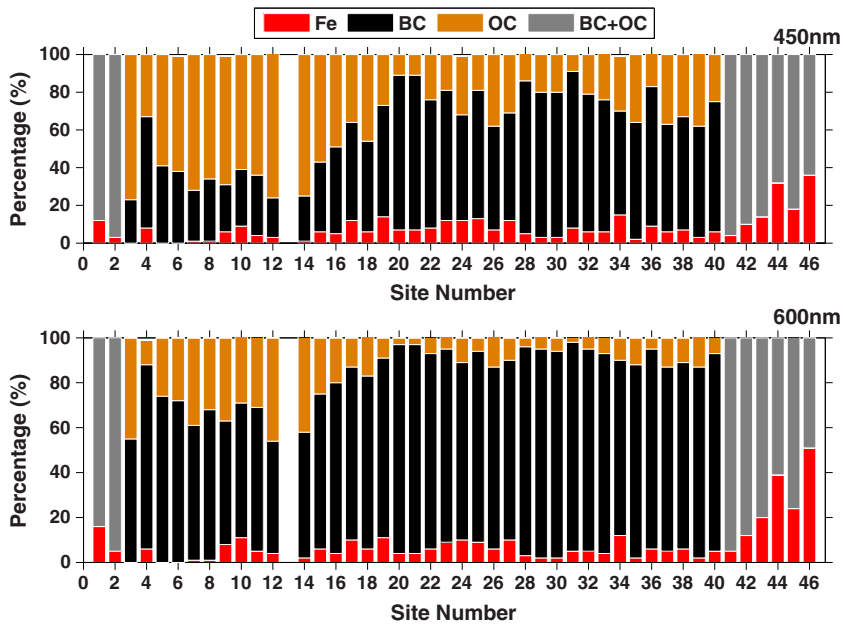

Figure 11. Relative contributions to total absorption optical depth by BC, OC, and Fe oxide (assumed to be in the form of goethite) for surface stirred snow samples (see Table 3).

burning or open burning. A more comprehensive chemical analysis is required to separate contributions from these sources; such an analysis is underway.

[54] The fractional contributions to absorption by BC, OC, and Fe at 450 and 600 nm are shown in Figure 11, and concentrations of BC and iron are given in Table 3. The fraction of light absorption due to Fe (assumed to be in the form of goethite) is ~30% in the Qilian Mountains. Elsewhere, BC and OC dominate the absorption, with Fe oxides contributing <10% to absorption (Figure 11) even though the Fe concentrations are as high at many of these sites as they are in the Qilian Mountains (Table 3). While we are assuming that Fe in snow is overwhelmingly from MD, it is possible that some of the Fe in snow is from industrial emissions (e.g. smelters, fly ash), even though our measurements were generally made >50 km from industrial activities. Concentrations of all particulate light absorbers are markedly lower at sites 21–24 than anywhere else (Table 3), but the relative contributions to absorption by BC, OC, and Fe appear to be fairly consistent for sites 15–40 (Figure 11)—that is, for the sites east of 117ºE (Figure 1). In this region, OC plays a notably smaller role in particulate light absorption than at the more western sites. For the western sites (3–14) of region 2, BC and OC play roughly comparable roles in light absorption. Emissions from biomass and biofuel combustion generally produce aerosol with a higher OC:BC ratio than does FF combustion [*Bond et al*., 2004], so this would be consistent with stronger contributions from biomass/biofuel burning in the more rural central north China and stronger contributions from FF burning in the more urban and industrial northeast China. However, since the source of OC could be soil, this difference could also be attributed to the relative roles of combustion aerosol and soil in snow particulate light absorption.

[55] Relative contributions to particulate light absorption vary with wavelength due to the differences in the spectral absorption properties of BC, OC, and Fe oxides. In apportioning absorption, we have used absorption Ångström exponents for BC, OC, and Fe oxide of 1.1, 6, and 3, so that at shorter wavelengths Fe and, especially, OC play a stronger role in light absorption (Figure 11). While the selected absorption Ångströms may not reflect the true spectral absorption properties of these constituents in the snow, $\AA$ for both Fe oxides and organics have been consistently found to be higher than that for BC, so accounting for their presence in snow is critical, especially when albedo effects over the whole spectrum are considered.

Table 3. Mass Concentrations of BC and Fe for the Stirred Snow Samples for Each Site Where Fe Data Are Available

	Snow Depth				
	Top	Bottom	C_{BC}^{equiv}	C_{BC}^{est}	C_{Fe}
Site	(cm)	(cm)	ng/g	ng/g	ng/g
1	0	3	2900	—	1600
2	0	4	3000	—	500
	0	4	1600	—	40
3	0	5	2700	910	20
4	0	3	2700	—	1000
5	0	5	2400	1200	60
6	0	5	3100	1400	50
7	10	20	2900	980	110
8	20	30	560	240	30
9	0	4	1400	430	430
10	0	4	360	130	150
11	5	10	1600	620	330
12	0	5	2500	640	340
13	3	8	—	—	2400
14	0	3	18,000	5300	1100
15	0	3	1800	800	490
16	0	2	6400	3500	1500
17	0	6	710	490	340
18	0	3	2000	1100	650
19	0	4	710	450	430
20	0	3	330	270	80
21	0	4	140	120	30
22	0	3	110	80	30
23	0	2	130	90	50
24	0	1	200	120	90
25	6	10	200	140	90
26	0	2	1000	620	300
27	0	4	1000	620	500
28	0	5	2400	1900	480
29	0	1.5	8300	6600	970
30	0	1	5600	4500	780
31	0	1	1600	1400	550
32	0	1	2100	1600	590
33	0	3	1600	1200	370
34	0	2	3600	2200	2500
35	0	2	3600	2500	440
36	0	4	1300	980	510
37	0	3	1700	1000	470
38	0	3	1700	1100	250
	3	6	2800	1900	1200
39	0	2	1600	1100	300
	3	5	1600	990	90
40	0	1	840	610	210
41	0	3	3900	—	700
42	0	2	1200	—	550
43	0	5	2700	—	1900
44	0	2	390	—	500
	0	1	420	—	600
45	0	2	420	—	540
	0	2	330	—	180
	0	1	610	—	420
46	0	4	600	—	950

3.5. Visual vs. Photometric Determination of BC Concentrations

[56] Concentrations of snow BC can be estimated by visually comparing loaded filters against the standard filters used in the ISSW calibration [*Grenfell et al*., 2011; *Huang et al*., 2011]. Visual estimates are made by placing the filters on a white background and comparing the color and darkness of the exposed area on the field samples to that on the standards. The standards are made from pure BC, so they range from lighter to darker shades of gray. The China 2010 field filters, however, vary in color from gray to brown to orange brown, depending on the contributions to absorption by BC vs. OC vs. Fe oxides. When light absorption is dominated by non-BC absorbers, the filters appear less gray and more brown or orange. In this case, it is not possible to visually separate the contribution to absorption by BC. Thus, visual estimates were made only for filters from regions where absorption appeared to be dominated by BC (i.e., the filters were more gray than brown) [*Huang et al*., 2011, Figure 5]. However, even in these cases a non-negligible part of the absorption is due to non-BC constituents (Figure 11), so the visual estimate, $C_{BC,vis}$, is an estimate of the equivalent BC loading that would be needed to explain the total filter darkening, including both BC and non-BC

components. This visual estimate of the loading is converted to a concentration based on filter-exposed area and the mass of water passed through the filter, identical to the conversion of ISSW-measured filter loading to snow concentration [*Grenfell et al.*, 2011]. Thus, the comparable value from the ISSW measurements is C_{BC}^{equiv}.

[57] Visual estimates of snow BC content were reported by *Huang et al.* [2011] for samples in regions 3 and 4 (sites 20–40) of the China 2010 field campaign and compared to snow BC concentrations from the model study of *Flanner et al.* [2009]. The visual estimates reported by *Huang et al.* [2011] converted the filter loading to a snow concentration using a fixed value for the filter-exposed area. The values of $C_{BC,vis}$ reported here are calculated using exposed areas as measured for each filter, resulting in visual estimates that are $17 \pm 9\%$ higher than those reported by *Huang et al.* [2011].

[58] Figure 12 compares the visual estimates, $C_{BC,vis}$, to C_{BC}^{equiv} from the ISSW measurement for sites 20–40. $C_{BC,vis}$ is systematically lower than C_{BC}^{equiv}, on average, by 54%. In contrast, *Grenfell et al.* [2011] show a comparison of $C_{BC,vis}$ and C_{BC}^{equiv} spanning a range of about 5–500 ng g^{-1} for snow samples from one expedition in Russia [*Grenfell et al.*, 2011, Figure 10]. Differences lie within bounds of uncertainty that span a factor of 2 and there is no apparent systematic bias in the values of $C_{BC,vis}$. The reason for the bias in the visual estimates of the China 2010 field filters vs. those from the expedition reported by *Grenfell et al.* [2011] is not known.

3.6. Comparison of Measured and Modeled Snow BC Concentrations

[59] *Huang et al.* [2011] reported that the modeled values of surface snow BC concentrations from the *Flanner et al.* [2009] study were, on average, 10% higher than the visually estimated surface snow concentrations from the China 2010 field campaign sites 20–40. Here we present an update to that comparison using estimated BC concentrations, C_{BC}^{est}, from sites 3–46. The average C_{BC}^{est} from the top 5 cm at each field site is compared with the average of the monthly average values from January and February for the top 2 cm of snow from the Flanner et al. model study.

[60] Ultimately of interest is radiative forcing by BC in snow, which is a function of the reduction in snow albedo. Albedo reduction, in turn, depends on snow BC mass mixing ratios and the MAE of a given quantity of BC. BC has a mid-visible (550 nm) MAE of 7.5 m^2 g^{-1} in the model study [*Flanner et al.*, 2009], whereas our BC masses are an equivalent mass assuming a 550 nm MAE of 6.3 m^2 g^{-1}. To make the two sets of snow BC concentrations comparable, we divide the values of C_{BC}^{est} given in Tables 1–3 by a factor of 1.19 to get the concentration of BC in snow that would be given by our optical measurements if the MAE of BC is, in fact, 7.5 m^2 g^{-1}.

[61] The measured values in this comparison are for the settled samples and so do not include contributions to absorption by very coarse-grained ($> \sim 10\,\mu$m diameter) particles from local soil mixed into the snow. This makes a more direct comparison with the modeled quantity, which also does not include this contribution to snow particulate light absorption. However, we remind the reader that in some regions these very coarse-grained particles increase total particulate light absorption by a factor of 1.5–3.0 or greater at some locations ($R_{settle,stir}$ in Table 1). Accurate representation of ambient snow albedo reduction therefore must account for these particles. Furthermore, the albedo reduction for a given concentration of BC is lower for snow that has a significant amount of particulate absorption due to soil particles than it is for a clean snowpack, so it consequently has a smaller radiative forcing.

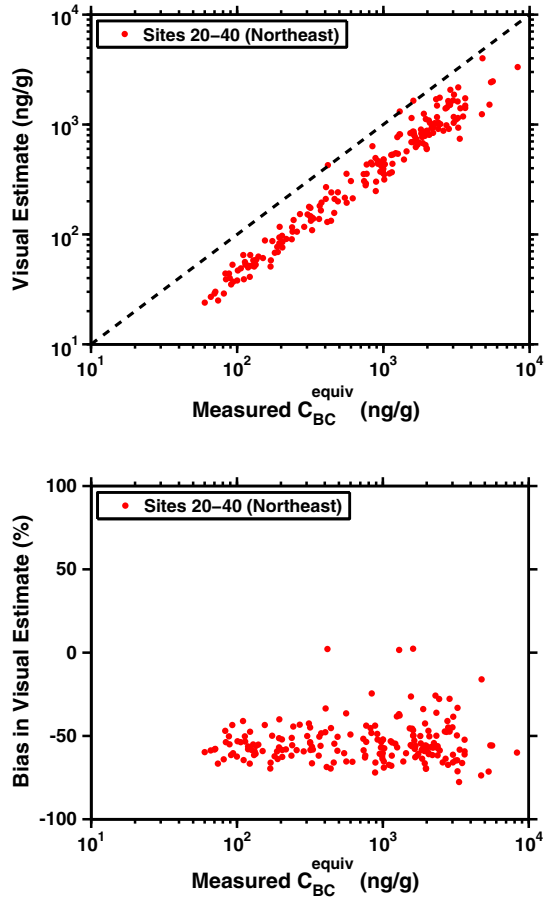

Figure 12. Bias in the visual estimate of equivalent BC concentrations, $C_{BC,vis}$, when compared to C_{BC}^{equiv} from the spectrophotometer measurements. Approximately 17% of the low bias in $C_{BC,vis}$ can be attributed to use of an incorrect filter-exposed area.

[62] The comparison (Figure 13) is shown as a function of longitude for central China (region 2; sites 3–19) and as a function of latitude for sites in northeast China (regions 3 and 4; sites 20–40). There are significant disagreements in the measured and modeled snow BC concentrations at individual sites in region 2, but over the region as a whole there is no apparent systematic bias in the modeled vs. measured concentrations. Along the north border of China near Siberia and in the industrial northeast of China, the model and measurements both show a steep drop-off in BC content with latitude, from ~1000 ng g^{-1} at 41–46°N to <100 ng g^{-1} north of 50°N. For sites 26–36 (from ~44.5°N to ~49.5°N; Figure 13a), modeled BC concentrations are systematically lower than the measured value, on average, by a factor of 0.58. North and south of these sites within region 2, there are again significant disagreements in snow BC concentrations at some sites, but no apparent low or high bias.

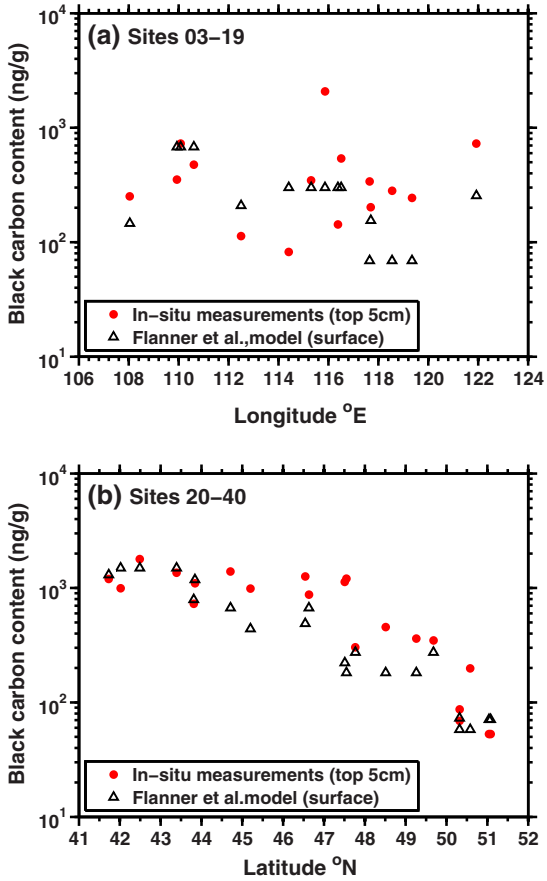

Figure 13. Comparison of measured (red dots) and modeled (black triangles) snow BC concentrations (a) for north-central China (region 2) as a function of longitude and for (b) northeastern China (regions 3 and 4) as a function of latitude. The measured values, C_{BC}^{est}, are for the top 5 cm of the snowpack and have been scaled down by a factor of 1.19 to account for the difference in the mass absorption efficiency of BC in the measurements ($6.3\ m^2\ g^{-1}$) vs. that used in the model ($7.5\ m^2\ g^{-1}$). The model values were provided by M. Flanner and reflect concentrations in the top 2 cm of the snowpack in the study of *Flanner et al.* [2009].

[63] This comparison is for snow BC concentrations only. As discussed earlier, non-BC constituents make significant, and sometimes dominant, contributions to snow particulate light absorption (e.g., Figure 11). In region 1, contributions by local soil appear to dominate absorption so strongly that the reduction in snow albedo due to BC may not significantly alter the surface energy budget, though the contribution is still positive (section 3.1.1). The model study of *Flanner et al.* [2009] includes snow darkening by dust, but only by dust transported at regional scales. The contribution by very local soil mixing into the snow via mechanical disturbance or wind transport over less than a few kilometers is not accounted for in this or other global-scale models and many model studies neglect dust (and other non-BC absorbers) in snow altogether. Testing of model representation of absorption by non-BC light absorbing impurities is also critical for knowing whether the models accurately represent reductions in surface albedo due to BC in snow. Also important to accurate calculations of surface albedo reductions by BC in snow is accurate representation of snow cover. As noted in section 3.1.1 and depicted in Figure 2f, snow cover in region 1 was extremely thin and patchy. In region 2 (section 3.1.2), snow cover was also thin and, in places, patchy. These critical comparisons of contributions by non-BC light-absorbing particulates to snow albedo reduction and a comparison of true versus modeled snow cover are left for later studies.

4. Discussion and Conclusions

[64] The large-area field campaign across north China in 2010 crossed regions with differing climatologies and sources of light-absorbing particulates to the snow. Within each of four regions, we analyze for light-absorbing particles (BC, OC, and dust) in snow based on optical and chemical measurements. In the arid Qilian Mountains, snow cover was thin and the land surface lacking vegetation so that local soil and MD from nearby deserts was easily mobilized and mixed with the snow. In this region, the snow particulate light absorption was dominated by local soil and dust. In any case, there was so little snow cover in this area that radiative forcing by impurities in snow was probably negligible. To the north and east, in the Inner Mongolian grasslands, snow cover was still thin, but was more complete than in the Qilian Mountains. Although BC was considered as an important contributor to snowpack light absorption, it appeared that local soil and/or desert dust transported from north China deserts also played a strong role in snow total particulate light absorption. Moving from the central grasslands eastward to northeast China along the Mongolian and Siberian borders, the role of non-BC absorbers decreased steadily and BC became the dominant absorber. The land was fully snow covered and the snowpack was deeper, so local soil could not readily mix with the snow, and the region is farther from the deserts of central and western China. The spectral absorption of the snow particulate light absorption in eastern north China is consistent with FF sources, and here it appears that local soil and desert dust do not have a strong influence in snowpack albedo reduction. BC emission sources in China are strongest in far eastern China ~30ºN–40ºN, immediately south of the area of our northeast China snow sampling. This is consistent with an observed strong north-south gradient in snow BC concentrations: Some of the lowest values of the campaign were in the far north of northeast China, and some of the highest values of the campaign in the southernmost sampling sites of northeast China. Typical surface concentrations, C_{BC}^{est}, in the far northeast correspond to reductions in pure snow albedo of ~1–6%, whereas typical concentrations in the latter to albedo reductions of ~5–20%, depending on snow grain size [*Warren and Wiscombe*, 1985].

[65] In a comparison with one global climate model, the model and measurement show general agreement on the spatial gradients in snow BC concentrations. There does not appear to be any gross bias in the model values, though at any given site there are often larger disagreements in snow BC concentrations. This highlights the importance of geographically broad surveys when testing regional to global scale models. Also important would be capturing interannual variability, which is not done here.

[66] Reported values of snow BC concentration and attribution of absorption to non-BC absorbers rests on assumptions

about the optical characteristics of filtered snow meltwater samples. As discussed above, recent comparisons of the method used here (ISSW spectrophotometer) with an SP2 on water samples with gravimetrically determined concentrations of BC and BC/dust mixtures indicate that the ISSW estimates of snow BC concentrations may have significant (up to a factor of 3) high biases when BC is mixed with dust and other particulate matter. Therefore, the snow BC concentrations presented here should be treated as upper bounds on snow BC. However, the measurement of the spectral properties of absorption is robust and can be used directly to quantify total snowpack particulate absorption. Furthermore, strong spectral dependence to the absorption is a clear indicator that non-BC absorbers are significantly influencing total light absorption, so that both BC and non-BC absorbers must be considered to accurately represent snowpack albedo reduction.

[67] **Acknowledgments.** This work was supported by the National Science Foundation of China under Grants 41175134 and 41105110, the Fundamental Research Funds for the Central Universities (lzujbky-2010-k06), and the U.S. Environmental Protection Agency EPA-G2010-STAR under grant number 83503801. The authors thank Rudong Zhang, Hao Ye, and Wu Zhang of Lanzhou University and Stephen Warren of the University of Washington for their assistance in field sampling. The authors thank Dean Hegg, Stephen Warren and Qiang Fu of the University of Washington Department of Atmospheric Sciences for their discussions and assistance with iron analyses (Dean Hegg) and for computing the down-welling solar radiation spectra used in Figure 4 (Qiang Fu). The authors thank Thomas C. Grenfell, who built the ISSW instrument used to measure the concentration of BC and other light-absorbing particles in snow in the lab of the University of Washington Department of Atmospheric Sciences. The authors thank Mark Flanner (University of Michigan) for providing the NCAR CAM 3.1 model fields of snow BC.

References

Adachi, K., and P. R. Buseck (2008), Internally mixed soot, sulfates, and organic matter in aerosol particles from Mexico City, *Atmos. Chem. Phys.*, *8*, 6469–6481, doi:10.5194/acp-8-6469-2008.

Alfaro, S. C., S. Lafon, J. L. Rajot, P. Formenti, A. Gaudichet, and M. Maille (2004), Iron oxides and light absorption by pure desert dust: An experimental study, *J. Geophys. Res.*, *109*, D08208, doi:10.1029/2003JD004374.

Andreae, M. O., and A. Gelencsér (2006), Black carbon or brown carbon? The nature of light-absorbing carbonaceous aerosols, *Atmos. Chem. Phys.*, *6*, 3131–3148, doi:10.5194/acp-6-3131-2006.

Armalis, S. (1999), Wet deposition of elemental carbon in Lithuania, *Sci. Total Environ.*, *239*, 89–93, doi:10.1016/S0048-9697(99)00288-0.

Bedidi, A., and B. Cervelle (1993), Light scattering by spherical particles with hematite and goethitelike optical properties: Effect on water impregnation, *J. Geophys. Res.*, *98*, 11,941–11,952, doi:10.1029/93JB00188.

Bergstrom, R. W., P. B. Russell, and P. Hignett (2002), Wavelength dependence of the absorption of black carbon particles: Predictions and results from the TARFOX experiment and implications for the aerosol single scattering albedo, *J. Atmos. Sci.*, *59*, 567–577, doi:10.1175/1520-0469.

Bergstrom, R. W., P. Pilewskie, P. B. Russell, J. Redemann, T. C. Bond, P. K. Quinn, and B. Sierau (2007), Spectral absorption properties of atmospheric aerosols, *Atmos. Chem. Phys.*, *7*, 5937–5943, doi:10.5194/acp-7-5937-2007.

Bond, T. C., M. Bussemer, B. Wehner, S. Keller, R. J. Charlson, and J. Heintzenberg (1999), Light absorption by primary particle emissions from a lignite burning plant, *Environ. Sci. Technol.*, *33*, 3887–3891, doi:10.1021/es9810538.

Bond, T. C. (2001), Spectral dependence of visible light absorption by carbonaceous particles emitted from coal combustion, *Geophys. Res. Lett.*, *28*(21), 4075–4078, doi:10.1029/2001GL013652.

Bond, T. C., D. G. Streets, K. F. Yarber, S. M. Nelson, J.-H. Woo, and Z. Klimont (2004), A technology-based global inventory of black and organic carbon emissions from combustion, *J. Geophys. Res.*, *109*, D14203, doi:10.1029/2003JD003697.

Bond, T. C., and R. W. Bergstrom (2006), Light absorption by carbonaceous particles: An investigative review, *Aerosol Sci. Tech.*, *40*, 27–67, doi:10.1080/02786820500421521.

Bond, T. C., G. Habib, and R. W. Bergstrom (2006), Limitations in the enhancement of visible light absorption due to mixing state, *J. Geophys. Res.*, *111*, D20211, doi:10.1029/2006JD007315.

Cachier, H., and M. H. Pertuisot (1994), Particulate carbon in Arctic ice, *Anal. Mag.*, *22*, 34–37.

Cadle, S. H., and J. M. Dasch (1988), Wintertime concentrations and sinks of atmospheric particulate carbon at a rural location in northern Michigan, *Atmos. Environ.*, *22*(7), 1373–1381, doi:10.1016/0004-6981(88)90162-X.

Chen, Y., and T. C. Bond (2010), Light absorption by organic carbon from wood combustion, *Atmos. Chem. Phys.*, *10*, 1773–1787, doi:10.5194/acp-10-1773-2010.

Chýlek, P., V. Strivastava, L. Cahenzli, R. G. Pinnick, R. L. Dod, T. Novakov, T. L. Cook, and B. D. Hinds (1987), Aerosol and graphitic carbon content of snow, *J. Geophys. Res.*, *92*(D8), 9801–9809, doi:10.1029/JD092iD08p09801.

Chýlek, P., B. Johnson, P. A. Damiano, K. C. Taylor, and P. Clement (1995), Biomass burning record and black carbon in the GISP2 Ice Core, *Geophys. Res. Lett.*, *22*(2), 89–92, doi:10.1029/94GL02841.

Clarke, A. D., and K. J. Noone (1985), Soot in the Arctic snowpack: A cause for perturbations in radiative transfer, *Atmos. Environ.*, *19*(12), 2045–2053, doi:10.1016/0004-6981(85)90113-1.

Clarke, A., C. McNaughton, V. Kapustin, Y. Shinozuka, S. Howell, J. Dibb, J. Zhou, B. Anderson, V. Brekhovskikh, H. Turner (2007), Biomass burning and pollution aerosol over North America: Organic components and their influence on spectral optical properties and humidification response, *J. Geophys. Res.*, *112*, D12S18, doi:10.1029/2006JD007777.

Dasch, J. M., and S. H. Cadle (1989), Atmospheric carbon particles in the Detroit urban area: Wintertime sources and sinks, *Aerosol Sci. Tech.*, *10*(2), 236–248, doi:10.1080/02786828908600508.

Doherty, S. J., S. G. Warren, T. C. Grenfell, A. D. Clarke, and R. E. Brandt (2010), Light-absorbing impurities in Arctic snow, *Atmos. Chem. Phys.*, *10*, 11,647–11,680, doi:10.5194/acp-10-11647-2010.

Fan, Q. Y., J. He, H. Xue, C. Lü, Y. Sun, L. Shen, Y. Liang, and S. Bai (2008), Heavy metal pollution in the Baotou section of the Yellow River, China, *Chem. Spec. Bioavailab.*, *20*, 65–76, doi:10.3184/095422908X322824.

Fialho, P., A. D. A. Hansen, and R. E. Honrath (2005), Absorption coefficients by aerosols in remote areas: A new approach to decouple dust and black carbon absorption coefficients using seven-wavelength Aethalometer data, *J. Aerosol Sci.*, *36*, 267–282, doi:10.1016/j.jaerosci.2004.09.004.

Fialho, P., M. C. Freitas, F. Barata, B. Vieira, A. D. A. Hansen, and R. E. Honrath (2006), The Aethalometer calibration and determination of iron concentration in dust aerosols, *Aerosol Sci.*, *37*, 1497–1506, doi:10.1016/j.jaerosci.2006.03.002.

Fily, M., B. Bourdelles, J. P. Dedieu, and C. Sergent (1997), Comparison of in situ and Landsat Thematic Mapper derived snow grain characteristics in the alps, *Remote Sens. Environ.*, *59*, 452–460, doi:10.1016/S0034-4257(96)00113-7.

Flanner, M. G., C. S. Zender, J. T. Randerson, and P. J. Rasch (2007), Present-day climate forcing and response from black carbon in snow. *J. Geophys. Res.*, *112*, D11202, doi:10.1029/2006JD008003.

Flanner, M. G., C. S. Zender, P. G. Hess, N.M. Mahowald, T. H. Painter, V. Ramanathan, and P. J. Rasch (2009), Springtime warming and reduced snow cover from carbonaceous particles. *Atmos. Chem. Phys.*, *9*, 2481–2497, doi:10.5194/acp-9-2481-2009.

Forsström, S., J. Ström, C. A. Pedersen, E. Isaksson, and S. Gerland (2009), Elemental carbon distribution in Svalbard snow, *J. Geophys. Res.*, *114*, D19112, doi:10.1029/2008JD011480.

Grenfell, T. C., B. Light, and M. Sturm (2002), Spatial distribution and radiative effects of soot in the snow and sea ice during the SHEBA experiment, *J. Geophys. Res.*, *107*, 8032, doi:10.1029/2000JC000414.

Grenfell, T. C., S. J. Doherty, A. D. Clarke, and S. G. Warren (2011), Light absorption from particulate impurities in snow and ice determined by spectrophotometric analysis of filters. *Appl. Opt.*, *50*, 2037–2048, doi:10.1364/AO.50.002037.

Gu, Y., K. N. Liou, W. Chen, and H. Liao (2010), Direct climate effect of black carbon in China and its impact on dust storms, *J. Geophys. Res.*, *115*, D00K14, doi:10.1029/2009JD013427.

Guo, H., M. Xu, and Q. Hu (2010), Changes in near-surface wind speed in China: 1969–2005 [online], *Int. J. Climatatol.*, doi:10.1002/joc.2091.

Hagler, G. S. W., M. H. Bergin, E. A. Smith, and J. E. Dibb (2007a), A summer time series of particulate carbon in the air and snow at Summit, Greenland, *J. Geophys. Res.*, *112*, D21309, doi:10.1029/2007JD008993.

Hagler, G. S. W., M. H. Bergin, E. A. Smith, J. E. Dibb, C. Anderson, and E. J. Steig (2007b), Particulate and water-soluble carbon measured in recent snow at Summit, Greenland, *Geophys. Res. Lett.*, *34*, L16505, doi:10.1029/2007GL030110.

Hansen, J., and L. Nazarenko (2004), Soot climate forcing via snow and ice albedos, *Proc. Natl. Acad. Sci.*, *101*, 423–428, doi:10.1073/pnas.2237157100.

Hansen, J., M. Sato, R. Ruedy, L. Nazarenko, A. Lacis, G. A. Schmidt, G. Russell, I. Aleinov, M. Bauer, and S. Bauer (2005), Efficacy of climate forcings, *J. Geophys. Res.*, *110*, D18104, doi:10.1029/2005JD005776.

Hegg, D. A., S. G. Warren, T. C. Grenfell, S. J. Doherty, T. V. Larson, and A. D. Clarke (2009), Source attribution of black carbon in Arctic snow, *Environ. Sci. Technol.*, *43*, 4016–4021, doi:10.1021/es803623f.

Hegg, D. A., S. G. Warren, T. C. Grenfell, S. J. Doherty, and A. D. Clarke (2010), Sources of light-absorbing aerosol in arctic snow and their seasonal variation, *Atmos. Chem. Phys.*, *10*, 10,923–10,938, doi:10.5194/acp-10-10923-2010.

Hoffer, A., A. Gelencsér, P. Guyon, G. Kiss, O. Schmid, G. P. Frank, P. Artaxo, and M. O. Andreae (2006), Optical properties of humic-like substances (HULIS) in biomass-burning aerosols, *Atmos. Chem. Phys.*, *6*, 3563–3570, doi:10.5194/acp-6-3563-2006.

Huang, J., P. Minnis, Y. Yi, Q. Tang, X. Wang, Y. Hu, Z. Liu, K. Ayers, C. Trepte, and D. Winker (2007), Summer dust aerosols detected from CALIPSO over the Tibetan Plateau, *Geophys. Res. Lett.*, *34*, L18805, doi:10.1029/2007GL029938.

Huang, J., P. Minnis, B. Chen, Z. Huang, Z. Liu, Q. Zhao, Y. Yi, and J. K. Ayers (2008), Long-range transport and vertical structure of Asian dust from CALIPSO and surface measurements during PACDEX, *Geophys. Res. Lett.*, *113*, D23212, doi:10.1029/2008JD010620.

Huang, J., P. Minnis, H. Yan, Y. Yi, B. Chen, L. Zhang, and J. K. Ayers (2010), Dust aerosol effect on semi-arid climate over Northwest China detected from A-Train satellite measurements, *Atmos. Chem. Phys.*, *10*, 12,465–12,495, doi:10.5194/acpd-10-12465-2010.

Huang, J., Q. Fu, W. Zhang, X. Wang, R. Zhang, H. Ye, and S. Warren (2011), Dust and black carbon in seasonal snow across northern China, *Bull. Amer. Meteor. Soc.*, *92*, 175–181, doi:10.1175/2010BAMS3064.1.

Intergovernmental Panel on Climate Change (2007), Climate change 2007: The physical science basis, Contribution of Working Group I to the Fourth Assessment Report of the Intergovernmental Panel on Climate Change, edited by S. Solomon, D. Qin, M. Manning, Z. Chen, M. Marquis, K. B. Averyt, M. Tignor, and H. L. Miller, 996 pp., Cambridge Univ. Press, New York.

Jacobson, M. Z. (2004), Climate response of fossil fuel and biofuel soot, accounting for soot's feedback to snow and sea ice albedo and emissivity, *J. Geophys. Res.*, *109*, D21201, doi:10.1029/2004JD004945.

Ji, J. F., W. Balsam, J. Chen, and L. W. Liu (2002), Rapid and quantitative measurement of hematite and goethite in the Chinese loess-paleosol sequence by diffuse reflectance spectroscopy, *Clays Clay Miner.*, *50*, 208–216. doi:10.1346/000986002760832801.

Kirchstetter, T. W., T. Novakov, and P. V. Hobbs (2004), Evidence that the spectral dependence of light absorption by aerosols is affected by organic carbon, *J. Geophys. Res.*, *109*, D21208, doi:10.1029/2004JD004999.

Koch, D., S. Menon, A. Del Genio, R. Ruedy, I. Alienov, and G. A. Schmidt (2009a), Distinguishing aerosol impacts on climate over the past century, *J. Clim.*, *22*, 2659–2677, doi:10.1175/2008JCLI2573.1.

Koch, D., M. Schulz, S. Kinne, C. McNaughton, J. R. Spackman, Y. Balkanski, S. Bauer, T. Berntsen, T. C. Bond, and O. Boucher (2009b), Evaluation of black carbon estimations in global aerosol models, *Atmos. Chem. Phys.*, *9*, 9001–9026, doi:10.5194/acp-9-9001-2009.

Kopacz, M., D. L. Mauzerall, J. Wang, E. M. Leibensperger, D. K. Henze, and K. Singh (2011), Origin and radiative forcing of black carbon transported to the Himalayas and Tibetan Plateau, *Atmos. Chem. Phys.*, *11*, 2837–2852, doi:10.5194/acp-11-2837-2011.

Lack, D. A., and C. D. Cappa (2010), Impact of brown and clear carbon on light absorption enhancement, single scatter albedo, and absorption wavelength dependence of black carbon, *Atmos. Chem. Phys.*, *10*, 4207–4220, doi:10.5194/acp-10-4207-2010.

Lafon, S., J. L. Rajot, S. C. Alfaro, and A. Gaudichet (2004), Quantification of iron oxides in desert aerosol, *Atmos. Environ.*, *38*, 1211–1218, doi:10.1016/j.atmosenv.2003.11.006.

Lafon, S., I. N. Sokolik, J. L. Rajot, S. Caquineau, and A. Gaudichet (2006), Characterization of iron oxides in mineral dust aerosols: Implications for light absorption, *J. Geophys. Res.*, *111*, D21207, doi:10.1029/2005JD007016.

Liu Y., J. R. Sun, B. Yang (2009), The effects of black carbon and sulphate aerosols in China regions on East Asia monsoons, *Tellus B*, *61*, 642–656, doi:10.1111/j.1600-0889.2009.00427.x.

Lu, Z., Q. Zhang, and D. G. Streets (2011), Sulfur dioxide and primary carbonaceous aerosol emissions in China and India, 1996–2010, *Atmos. Chem. Phys.*, *11*, 9839–9864, doi:10.5194/acp-11-9839-2011.

Mao, C., J. Chen, X. Yuan, Z. Yang, W. Balsam, and J. Ji (2010), Seasonal variation in the mineralogy of the suspended particulate matter of the lower Changjiang River at Nanjing, China, *Clays Clay Miner.*, *58*(5), 691–706, doi:10.1346/CCMN.2010.0580508.

McConnell, J. R., R. Edwards, G. L. Kok, M. G. Flanner, C. S. Zender, E. S. Saltzman, J. R. Banta, D. R. Pasteris, M. M. Carter, and J. D. W. Kahl (2007), 20th-century industrial black carbon emissions altered arctic climate forcing, *Science*, *317*, 1381–1384, doi:10.1126/science.1144856.

Meloni, D., A. di Sarra, G. Pace, and F. Monteleone (2006), Aerosol optical properties at Lampedusa (Central Mediterranean). 2. Determination of single scattering albedo at two wavelengths for different aerosol types, *Atmos. Chem. Phys.*, *6*, 715–727, doi:10.5194/acp-6-715-2006.

Millikan, R. C. (1961), Optical properties of soot, *J. Opt. Soc. Am.*, *51*, 698–699, doi:10.1364/JOSA.51.000698.

Ming, J., H. Cachier, C. Xiao, D. Qin, S. Kang, S. Hou, and J. Xu (2008), Black carbon record based on a shallow Himalayan ice core and its climatic implications, *Atmos. Chem. Phys.*, *8*, 1343–1352, doi:10.5194/acp-8-1343-2008.

Ming, J., C. Xiao, H. Cachier, D. Qin, X. Qin, Z. Li, and J. Pu (2009), Black Carbon (BC) in the snow of glaciers in west China and its potential effects on albedos, *Atmos. Res.*, *92*, 114–123, doi:10.1016/j.atmosres.2008.09.007.

Müller, T., A. Schladitz, A. Massling, N. Kaaden, K. Kandler, and A. Wiedensohler (2009), Spectral absorption coefficients and imaginary parts of refractive indices of Saharan dust during SAMUM-1, *Tellus B*, *61*, 79–95, doi:10.1111/j.1600-0889.2008.00399.x.

Ogren, J. A., R. J. Charlson, and P. J. Groblicki (1983), Determination of elemental carbon in rainwater, *Anal. Chem.*, *55*(9), 1569–1572, doi:10.1021/ac00260a027.

Painter, T. H., A. P. Barrett, C. C. Landry, J. C. Neff, M. P. Cassidy, C. R. Lawrence, K. E. McBride, and G. L. Farmer (2007), Impact of disturbed desert soils on duration of mountain snow cover, *Geophys. Res. Lett.*, *34*, L12502, doi:10.1029/ 2007GL030284.

Prospero, J. M., P. Ginoux, O. Torres, S. E. Nicholson, and T. E. Gill (2002), Environmental characterization of global sources of atmospheric soil dust identified with the NIMBUS 7 Total Ozone Mapping Spectrometer (TOMS) absorbing aerosol product, *Rev. Geophys.*, *40*(1), 1002, doi:10.1029/20000GR000095.

Qian, Y., W. I. Gustafson, L. R. Leung, and S. J. Ghan (2009), Effects of soot-induced snow albedo change on snowpack and hydrological cycle in western United States based on weather research and forecasting chemistry and regional climate simulations, *J. Geophys. Res.*, *114*, D03108, doi:10.1029/2008JD011039.

Qian, Y., M. G. Flanner, L. R. Leung, and W. Wang (2011), Sensitivity studies of the impacts of Tibetan Plateau snowpack pollution on the Asian hydrologic cycle and monsoon climate, *Atmos. Chem. Phys.*, *11*, 1929–1948, doi:10.5194/acp-11-1929-2011.

Rosen, H., A. D. A. Hansen, L. Gundel, and T. Novakov (1978), Identification of the optically absorbing component in urban aerosols, *Appl. Opt.*, *17*, 3859–3861, doi:10.1364/AO.17.003859.

Schnaiter, M., H. Horvath, O. Möhler, K. H. Naumann, H. Saathoff, and O. W. Schöck (2003), UV-VIS-NIR spectral optical properties of soot and soot-containing aerosols, *J. Aerosol Sci.*, *34*, 1421–1444, doi:10.1016/S0021-8502(03)00361-6.

Schnaiter, M., C. Linke, O. Möhler, K. H. Naumann, H. Saathoff, R. Wagner, U. Schurath, and B. Wehner (2005), Absorption amplification of black carbon internally mixed with secondary organic aerosol, *J. Geophys. Res.*, *110*, D19204, doi:10.1029/2005JD006046.

Schnaiter, M., M. Gimmler, I. Llamas, C. Linke, C. Jäger, and H. Mutschke (2006), Strong spectral dependence of light absorption by organic carbon particles formed by propane combustion, *Atmos. Chem. Phys.*, *6*, 2981–2990, doi:10.5194/acp-6-2981-2006.

Schwarz, J. P., J. R. Spackman, R. S. Gao, L. A. Watts, P. Stier, M. Schulz, S. M. Davis, S. C. Wofsy, and D. W. Fahey (2010), Global-scale black carbon profiles observed in the remote atmosphere and compared to models, *Geophys. Res. Lett.*, *37*, L18812, doi:10.1029/2010GL044372.

Schwarz, J. P., S. J. Doherty, F. Li, S. T. Ruggiero, C. E. Tanner, A. E. Perring, R. S. Gao, and D. W. Fahey (2012), Assessing Single Particle Soot Photometer and Integrating Sphere/Integrating Sandwich Spectrophotometer measurement techniques for quantifying black carbon concentration in snow, *Atmos. Meas. Tech.*, *5*, 2581–2592, doi:10.5194/amtd-5-2581-2012.

Sergent, C., E. Pougatch, M. Sudul, and B. Bourdelles (1993), Experimental investigation of optical snow properties, *Ann. Glaciol.*, *17*, 281–287.

Sergent, C., C. Leroux, E. Pougatch, and F. Guirado (1998), Hemispherical-directional reflectance measurements of natural snows in the 0.9–1.45 μm spectral range: Comparison with adding-doubling modelling, *Ann. Glaciol.*, *26*, 59–63.

Shapiro, E. L., J. Szprengiel, N. Sareen, C. N. Jen, M. R. Giordano, and V. F. McNeill (2009), Light-absorbing secondary organic material formed by glyoxal in aqueous aerosol mimics, *Atmos. Chem. Phys.*, *9*, 2289–2300, doi:10.5194/acp-9-2289-2009.

Shindell, D., and G. Faluvegi (2009), Climate response to regional radiative forcing during the twentieth century, *Nat. Geosci.*, *2*, 294–300, doi:10.1038/ngeo473.

Sokolik, I. N., and O. B. Toon (1999), Incorporation of mineralogical composition into models of the radiative properties of mineral aerosol

from UV to IR wavelengths, *J. Geophys.*, *104*(D8), 9423–9444, doi:10.1029/1998JD200048.

van der Werf, G. R., J. T. Randerson, L. Giglio, G. J. Collatz, P. S. Kasibhatla, and A. F. Arellano, Jr. (2006), Interannual variability in global biomass burning emissions from 1997 to 2004, *Atmos. Chem. Phys.*, *6*, 3423–3441, doi:10.5194/acp-6-3423-2006.

Wake, C. P., and P. A. Mayewski (1994), Modern eolian dust deposition in central Asia, *Tellus B*, *46*, 220–233, doi:10.1034/j.1600-0889.1994.t01-2-00005.x.

Wang, X., J. P. Huang, M. X. Ji, and K. Higuchi (2008), Variability of East Asia dust events and their long-term trend, *Atmos. Environ.*, *42*, 3156–3165, doi:10.1016/j.atmosenv.2007.07.046.

Wang, X., J. P. Huang, R. D. Zhang, B. Chen, J. R. Bi (2010), Surface measurements of aerosol properties over northwest China during ARM China 2008 deployment, *J. Geophys. Res.*, *115*, D00K27, doi:10.1029/2009JD013467.

Warren, S. G., and W. Wiscombe (1980), A model for the spectral albedo of snow. II: Snow containing atmospheric aerosols, *J. Atmos. Sci.*, *37*, 2734–2745, doi:10.1175/1520-0469.

Warren, S. G., and W. J. Wiscombe (1985), Dirty snow after nuclear war, *Nature*, *313*, 467–470, doi:10.1038/313467a0.

Xu, B., T. Yao, X. Liu, and N. Wang (2006), Elemental and organic carbon measurements with a two-step heating-gas chromatography system in snow samples from the Tibetan Plateau, *Ann. Glaciol.*, *43*, 257–262, doi:10.3189/172756406781812122.

Xu, B. Q., M. Wang, D. R. Joswiak, J. J. Cao, T. D. Yao, G. J. Wu, W. Yang, and H. B. Zhao (2009), Deposition of anthropogenic aerosols in a southeastern Tibetan glacier, *J. Geophys. Res.*, *114*, D17209, doi:10.1029/ 2008JD011510.

Xu B. Q., J. J. Cao, D. R. Joswiak, X. Q. Liu, H. B. Zhao, and J. Q. He (2012), Post-depositional enrichment of black soot in snow-pack and accelerated melting of Tibetan glaciers, *Environ. Res. Lett.*, *7*, 014022. doi:10.1088/1748-9326/7/1/014022.

Yang, M., S. G. Howell, J. Zhuang, and B. J. Huebert (2009), Attribution of aerosol light absorption to black carbon, brown carbon, and dust in China-interpretations of atmospheric measurements during EAST-AIRE, *Atmos. Chem. Phys.*, *9*, 2035–2050, doi:10.5194/acp-9-2035-2009.

Ye H., R. D. Zhang, J. S. Shi, J. P. Huang, S. G. Warren, and Q. Fu (2012), Black carbon in seasonal snow across northern Xinjiang in northwestern China, *Environ. Res. Lett.*, *7*, 044002, doi:10.1088/1748-9326/7/4/044002.

Zhao, R. X., W. Guo, W. H. Sun, S. L. Xue, B. Gao, and W. Sun (2012), Distribution characteristic and assessment of soil heavy metal pollution around Baotou tailings in Inner Mongolia, China, *Adv. Mater. Res.*, *356–360*, 2730–2736, doi:10.4028/www.scientific.net/AMR.518-523.2068.